Risk-based Distributionally Robust Optimal Gas-Power Flow With Wasserstein Distance

Cheng Wang, *Member, IEEE*, Rui Gao, Wei Wei, *Senior Member, IEEE*, Miadreza Shafie-khah, *Senior Member, IEEE*, Tianshu Bi, *Senior Member, IEEE*, João P. S. Catalão, *Senior Member, IEEE*

***Abstract*—Gas-fired units and power-to-gas facilities provide pivotal backups for power systems with volatile renewable generations. The deepened system interdependency calls for elaborate consideration of network models of both natural gas and power systems, as well as uncertain factors. This paper proposes a data-driven distributionally robust optimization model for the optimal gas-power flow problem with uncertain wind generation. The concept of zonal line pack and line pack reserve are raised to topologically distinguish fuel suppliers of gas-fired units and ensure gas system operating security during reserve deployment. Wind power uncertainty is described by an ambiguity set, i.e., a family of candidate distributions around an empirical distribution in the sense of Wasserstein distance. A convex optimization based solution procedure is developed, which entails solving only second-order cone programs. Computational results validate the effectiveness of the proposed models and methods.**

***Index Terms*—Convex optimization, distributionally robust optimization, optimal gas-power flow, risk, Wasserstein distance.**

NOMENCLATURE

A. Sets and Indices

$t \in \mathcal{T}$	Time periods.
$n \in \mathcal{N}$	Non-gas units.
$g \in \mathcal{G}$	Gas-fired units.
$d_e \in \mathcal{D}_e$	Electricity loads.
$d_g \in \mathcal{D}_g$	Gas loads.
$w \in \mathcal{W}$	Wind farms.
$l_e \in \mathcal{L}_e$	Power transmission lines.
$l_g \in \mathcal{L}_g$	Gas pipelines.
$\mathcal{L}_g^c$	Gas active pipeline sets.
$i_g \in \mathcal{I}_g$	Gas network nodes.
$e \in \mathcal{E}$	Gas wells.
$s \in \mathcal{S}$	Samples of wind generation outputs.
$\mathcal{M}$	Ambiguity Set.
$\mathcal{P}$	The set of all probability distributions.
T/S	Number of time periods/samples.
N/G	Number of non-gas/gas-fired units.
L_e	Number of power transmission lines.

B. Parameters

f_n	Cost functions of non-gas units [$/MW].
f_n^+/f_n^-	Upward/downward regulation costs functions of non-gas units [$/MW].
$f_{l_g}^+/f_{l_g}^-$	Upward/downward regulation costs functions of line pack [$/(Sm$^3 \cdot$ h^{-1})].
Q_{et}	Gas production costs coefficients [$/Sm^3].
$p_{d_e t}$	Electricity demands [MW].
p_{wt}	Forecasting outputs of wind farms [MW].
π_{gl_e}/π_{nl_e}	Power transfer distribution factors of gas-fired/non-gas units [-].
$\pi_{wl_e}/\pi_{d_e l_e}$	Power transfer distribution factors of wind farms/electricity loads [-].
p_{l_e}	Capacity limits of power transmission lines [MW].
u_{gt}/u_{nt}	Operating status of gas-fired/non-gas units [-].
$\bar{p}_g/\underline{p}_g$	Upper/lower capacity limits of gas-fired units [MW].
$\bar{p}_n/\underline{p}_n$	Upper/lower capacity limits of non-gas units [MW].
P_g^+, P_g^-	Ramping limits of gas-fired units [MW/h].
P_n^+, P_n^-	Ramping limits of non-gas units [MW/h].
$\bar{q}_e/\underline{q}_e$	Production limits of gas wells [Sm$^3 \cdot$ h^{-1}].
$\bar{v}_{i_g}/\underline{v}_{i_g}$	Pressure limits of gas nodes [Pa].
$q_{d_g t}$	Gas demands [Sm$^3 \cdot$ h^{-1}].
η_g	Efficiency of gas-fired units [-].
σ	Electricity-to-gas conversion constant [Sm^3/(MWh)].
χ_{l_g}	Gas consumption coefficients [-].
ϕ_{l_g}	Weymouth equation coefficients [(Sm^3)^2/(Pa$\cdot$ h)^2].
ψ_{l_g}	Line pack coefficients [Sm^3/Pa].
$\gamma_{l_g}^c$	Compression factors of compressors [-].

This work was supported in part by the National Natural Science Foundation of China (51725702, 51627811, 51807059), and in part by the "111" project (B08013), and in part by the Fundamental Research Funds for the Central Universities (2018MS002). J. P. S. Catalão acknowledges the support by FEDER funds through COMPETE 2020 and by Portuguese funds through FCT, under Projects SAICT-PAC/0004/2015 - POCI-01-0145-FEDER-016434 and 02/SAICT/2017 - POCI-01-0145-FEDER-029803.

C. Wang and T. Bi are with the State Key Laboratory of Alternate Electrical Power System with Renewable Energy Sources, North China Electric Power University, Beijing 102206, China (e-mail: chengwang@ncepu.edu.cn, tsbi@ncepu.edu.cn).

R. Gao is with Department of Information, Risk, and Operations Management (IROM), McCombs School of Business, University of Texas at Austin, Austin, TX 78712, USA (e-mail: rui.gao@mccombs.utexas.edu).

W. Wei is with the State Key Laboratory of Power Systems, Department of Electrical Engineering, Tsinghua University, 100084 Beijing, China. (e-mail: wei-wei04@mails.tsinghua.edu.cn)

M. Shafie-khah is with INESC TEC, Porto 4200-465, Portugal (e-mail: miadreza@gmail.com).

J. P. S. Catalão is with the Faculty of Engineering of the University of Porto (FEUP) and INESC TEC, Porto 4200-465, Portugal, also with C-MAST, University of Beira Interior, Covilh 6201-001, Portugal, and also with INESC-ID, Instituto Superior Tcnico, University of Lisbon, Lisbon 1049-001, Portugal (e-mail: catalao@fe.up.pt).

$\bar{q}^c_{l_g}$	Maximal allowed gas in-flows of compressors [Sm^3/h].
$\bar{p}_w$	Installed capacities of wind farms [MW].
$\beta_w/\beta_{d_e}/\beta_{l_e}$	Penalties of wind power curtailment/electricity load shedding/line overload [$/MW].
θ	Radius of the Wasserstein ambiguity set [-].

C. Decision Variables

p_{gt}/p_{nt}	Outputs of gas-fired/non-gas units [MW].
q_{et}	Outputs of gas wells [$Sm^3 \cdot h^{-1}$].
$v_{i_g t}$	Pressure of gas nodes [Pa].
$q_{l_g t}$	Average flow of gas pipelines [$Sm^3 \cdot h^{-1}$].
$q^{in}_{l_g t}/q^{out}_{l_g t}$	In-/out-flows of gas pipelines [$Sm^3 \cdot h^{-1}$].
$m_{l_g t}$	Line pack [Sm^3].
r^+_{gt}, r^-_{gt}	Upward/downward reserves of gas-fired units [MW].
r^+_{nt}, r^-_{nt}	Upward/downward reserves of non-gas units [MW].
α_{gt}/α_{nt}	Reserve participation factors of gas-fired/non-gas units [-].
$m^{g,+}_{l_g t}/m^{g,-}_{l_g t}$	Line pack reserve purchased by gas-fired units [$Sm^3 \cdot h^{-1}$].
$\bar{m}_{l_g t}/\underline{m}_{l_g t}$	Upper/lower bounds of line pack [Sm^3].
$v^l_{l^1_g t}/v^h_{l^1_g t}$	Pressure bounds of head node of passive pipelines [Pa].

D. Random Variables

$\tilde{p}_{wt}$	Actual outputs of wind farms [MW].

I. Introduction

WITH the increasing share of gas-fired units in the electricity generation industry [1] as well as the promotion of the emerging power-to-gas technology globally [2], the integration of the power systems and the natural gas systems has entered a new era. Opportunities and benefits have been brought by the technical trend, yet the existence of challenges are undeniable. Inspiring works have been done and taken positive effects on smoothing and accelerating the gas-power integration from operation [3], planning [4] as well as market [5] perspectives, to name just a few.

As one of the most fundamental problems in the integrated gas-electric system operation, optimal gas-power flow (OGPF) has been widely discussed by the literature. The security constrained OGPF with steady-state gas flow model is proposed in [6], where the nonconvex Weymouth equation is approximated by a piecewise linear function, and the OGPF problem is cast as a mixed integer linear program (MILP). To incorporate the slow gas dynamics, also known as the line pack, which is described by partial differential equations, linear discrete approximation is employed in [7] and the OGPF is solved via an MILP. Though [6] and [7] have provided viable options for the OGPF problem, large-scale instances remain computational challenging, as the number of integer variables grows rapidly with growing system sizes. Recent OGPF works have leveraged more tractable convex optimization techniques by replacing the nonconvex Weymouth equations with relaxed but simpler constraints, such as linear ones [8] and second-order cones (SOCs) [9]. Nevertheless, these convex relaxation models are generally inexact and offer infeasible solutions. A sequential algorithm is proposed in [10] to enhance the feasibility of OGPF solutions, and a feasible and local solution can be refined in most occasions.

Beyond the deterministic OGPF formulations, tackling uncertainty is another important issue in OGPF, because of the increasing level of renewable generation in the integrated gas-electric systems. Scenario based stochastic program (SP) is used in [11] to capture the wind generation outputs uncertainty, where the coordinated scheduling of the gas-electric system is analyzed. In [12], uncertain wind generation outputs and demand are described by uncertainty sets, and the scheduling problem of the integrated energy system is formulated and solved based on robust optimization (RO). Inheriting advantages from both SP and RO, distributionally robust optimization (DRO) is developed recently, where a distributional uncertainty set is constructed, containing a family of candidate distributions for the uncertain data. Since DRO approaches are usually data-driven, it is less conservative than classical RO by explore the statistical properties, and makes no reference to the exact probability distribution [13]. Recently, DRO has been successfully applied to power system operation problems, such as unit commitment [14], reserve procurement [15], and optimal power flow [16], yet DRO based OGPF studies have not been reported so far.

In this paper, a risk-based OGPF model is proposed. It is built upon a data-driven distributionally robust framework that hedges against inexact probability distribution of wind power output, and referred to DROGPF for short. Compared with the existing works, the salient features of our work are:

1) In the proposed DROGPF model, the sum of operational cost and risk are minimized. The former consists of energy generation and reserve commitment costs; the latter incorporates penalties on load shedding, wind power curtailment and line overload. Randomness of wind generation outputs is modeled by a distributional uncertainty set, and the distance between candidate distributions and a reference distribution is no greater than a threshold in the sense of Wasserstein distance [17]; the reference distribution can be constructed from limited historical data, and can be inexact.

2) Inspired by [18], the concept of zonal line pack is proposed, which topologically defines the gas fuel suppliers for reserves provided by gas-fired units. Additional gas fuel constraints, called line pack reserve availability constraints, are included in the proposed DROGPF model so as to limit gas-fired reserves besides the regulation capability of gas-fired units. It offers a more practical way to analyze the impacts of reserve provision of gas-fired units on the gas system, as the dynamics in gas systems is relatively slow.

3) A second-order cone program (SOCP) based algorithm is developed to solve the proposed DROGPF problem. The computation time grows linearly with respect to the scale of the test system as well as the sample dataset, indicating the promising scalability of the proposed methods.

II. Mathematical Formulation

A. Deterministic OGPF

In this work, we assume there exists one utility who has fully control authority over both the electricity and gas systems, which is in line with the settings of [6], [7], [12], [19]. The mathematical formulation of the deterministic OGPF problem is given as below, where the direct current losses power flow model is adopted for the power system and the line pack effect in the gas system is considered:

$$\min_{\Phi} \sum_{t\in\mathcal{T}} \left(\sum_{n\in\mathcal{N}} f_n\left(p_{nt}\right) + \sum_{e\in\mathcal{E}} Q_{et} q_{et} \right) \tag{1a}$$

$$s.t. \sum_{g\in\mathcal{G}} p_{gt} + \sum_{n\in\mathcal{N}} p_{nt} + \sum_{w\in\mathcal{W}} p_{wt} = \sum_{d_e\in\mathcal{D}_e} p_{d_e t},\ \forall t\in\mathcal{T}, \tag{1b}$$

$$\Big| \sum_{g\in\mathcal{G}} \pi_{gl_e} p_{gt} + \sum_{n\in\mathcal{N}} \pi_{nl_e} p_{nt} + \sum_{w\in\mathcal{W}} \pi_{wl_e} p_{wt} - \sum_{d_e\in\mathcal{D}_e} \pi_{d_e l_e} p_{d_e t} \Big| \le p_{l_e},\ \forall l_e\in\mathcal{L}_e,\ \forall t\in\mathcal{T}, \tag{1c}$$

$$\begin{aligned} &u_{\{\cdot\}t}\underline{p}_{\{\cdot\}} \le p_{\{\cdot\}t} \le u_{\{\cdot\}t}\bar{p}_{\{\cdot\}}, \\ &\{\cdot\} = \{g,n\}, \forall n\in\mathcal{N}, \forall g\in\mathcal{G}, \forall t\in\mathcal{T}, \end{aligned} \tag{1d}$$

$$\begin{aligned} &p_{\{\cdot\}t} - p_{\{\cdot\},t+1} \le u_{\{\cdot\},t+1} P^{-}_{\{\cdot\}} + (1-u_{\{\cdot\},t+1})\bar{p}_{\{\cdot\}}, \\ &\{\cdot\} = \{g,n\}, \forall n\in\mathcal{N}, \forall g\in\mathcal{G}, \forall t\in\mathcal{T}, \end{aligned} \tag{1e}$$

$$\begin{aligned} &p_{\{\cdot\},t+1} - p_{\{\cdot\}t} \le u_{\{\cdot\}t} P^{+}_{\{\cdot\}} + (1-u_{\{\cdot\}t})\bar{p}_{\{\cdot\}}, \\ &\{\cdot\} = \{g,n\}, \forall n\in\mathcal{N}, \forall g\in\mathcal{G}, \forall t\in\mathcal{T}, \end{aligned} \tag{1f}$$

$$\underline{q}_e \le q_{et} \le \bar{q}_e,\ \forall e\in\mathcal{E},\ \forall t\in\mathcal{T}, \tag{1g}$$

$$\begin{aligned} &\sum_{e\in\Theta_e(i_g)} q_{et} - \sum_{d_g\in\Theta_{d_g}(i_g)} q_{d_g t} - \sum_{l_g\in\Theta_{l_g^1}(i_g)} q^{in}_{l_g t} = \\ &\sigma\cdot \sum_{g\in\Theta_g(i_g)} p_{gt}/\eta_g - \sum_{l_g\in\Theta_{l_g^2}(i_g)} (1-\chi_{l_g}) q^{out}_{l_g t}, \\ &\forall i_g\in\mathcal{I}_g,\ \forall t\in\mathcal{T}, \end{aligned} \tag{1h}$$

$$m_{l_g t} = \psi_{l_g}\left(v_{l_g^1 t} + v_{l_g^2 t}\right),\ \forall l_g\in\mathcal{L}_g,\ \forall t\in\mathcal{T}, \tag{1i}$$

$$m_{l_g t} = m_{l_g,t-1} + q^{in}_{l_g t} - q^{out}_{l_g t},\ \forall l_g\in\mathcal{L}_g,\ \forall t\in\mathcal{T}, \tag{1j}$$

$$q_{l_g t} = \left(q^{in}_{l_g t} + q^{out}_{l_g t}\right)/2,\ \forall l_g\in\mathcal{L}_g,\ \forall t\in\mathcal{T}, \tag{1k}$$

$$q_{l_g t}|q_{l_g t}| = \phi_{l_g}\left(\left(v_{l_g^1 t}\right)^2 - \left(v_{l_g^2 t}\right)^2\right),\ \forall l_g\in\mathcal{L}_g/\mathcal{L}^c_g,\ \forall t\in\mathcal{T}, \tag{1l}$$

$$v_{l_g^2 t} \le \gamma^c_{l_g} v_{l_g^1 t},\ \forall l_g\in\mathcal{L}^c_g,\ \forall t\in\mathcal{T}, \tag{1m}$$

$$0 \le q^{in}_{l_g t} \le \bar{q}^c_{l_g},\ \forall l_g\in\mathcal{L}^c_g,\ \forall t\in\mathcal{T}, \tag{1n}$$

$$\underline{v}_{i_g} \le v_{i_g t} \le \bar{v}_{i_g},\ \forall i_g\in\mathcal{I}_g, \forall t\in\mathcal{T}, \tag{1o}$$

$$\Phi = \{p_{gt}, p_{nt}, q_{et}, q^{in}_{l_g t}, q^{out}_{l_g t}, q_{l_g t}, m_{l_g t}, v_{i_g t}\}. \tag{1p}$$

In OGPF problem (1), (1a) represents the out-of-the-pocket costs of the integrated energy system, where the first and second terms depict the generation costs of non-gas units and gas production costs of gas wells, respectively [6], [7], [12]. The production costs of gas-fired units are included in the gas production costs by adding their fuel demands in nodal gas balancing conditions. (1b)-(1f) are power system related constraints, and (1g)-(1o) are gas system related constraints. Specifically, (1b) indicates the system-wide power balancing condition. (1c) gives the power flow limits on transmission lines. (1d) presents generation capacity limits for gas-fired and non-gas units. (1e) and (1f) are ramping down and up constraints for units, respectively. The outputs of gas wells are bounded by (1g). The nodal gas balancing conditions are depicted by (1h). (1i) defines the line pack within a pipeline, where the subscripts l_g^1 and l_g^2 represent the head and tail nodes of pipeline l_g, respectively. (1j) interprets the line pack dynamics [7]. (1k) depicts the average gas flow within a pipeline. Particularly, the pipelines with and without compressors are called active and passive pipelines, respectively. For active pipelines, the gas consumed by the compressors are reflected by χ_{l_g} ahead of the gas in-flow terms in (1h) [20]. (1l) is the Weymouth equation, which captures the relationship between the average gas flow and nodal pressures for a passive pipeline. (1m) and (1n) limit the compression ratio and gas flow of an active pipeline, respectively [21]. (1o) suggests the pressure limits at gas system nodes. (1p) collects all the decision variables for problem (1).

Due to the existence of the nonconvex Weymouth equation, problem (1) can hardly be solved by commercial solvers. Fortunately, the topologies of transmission-level gas networks are usually radial [22]. Moreover, according to gas system operation practice, the gas flow directions do not change intra-day [23]. Then, (1l) can be reduced as

$$\left(q_{l_g t}\right)^2 = \phi_{l_g}\left(\left(v_{l_g^1 t}\right)^2 - \left(v_{l_g^2 t}\right)^2\right), \tag{2a}$$

$$v_{l_g^1 t} \ge v_{l_g^2 t},\ \forall l_g\in\mathcal{L}_g/\mathcal{L}^c_g,\ \forall t\in\mathcal{T}, \tag{2b}$$

where we assume the notations of the initial and terminal nodes of l_g are consistent with the positive directions of gas flows. Note that (2) is still nonconvex. A convexification method will be introduced in Section III-A.

Remark 1: At the present stage, most existing coupled electricity-gas systems have two operating entities, who run the power system and the gas system, respectively. Nevertheless, several driving forces have been continuously promoting the integration of power-gas systems and might facilitate a unified entity who has operation authority for both power and gas systems in the near future, which are

- The deepening interdependency between power systems and gas systems. According to [1], the proportion of gas demand used for power generation over the total gas consumption has reached 40% globally in 2012 and will keep increasing in the next years. Meanwhile, quite a few power-to-gas (P2G) demonstration plants have been built worldwide, suggesting growing electricity demands from gas systems.
- Large-scale multi-energy utilities. Currently, there exists several large-scale multi-energy utilities who could provide multiple types of energy including gas and electricity to their customers, such as Pacific Gas & Electric and

Public Service Elec & Gas in the USA [24]. Their interests are to maximize the energy sales profits or minimize the energy supply costs.

- The potential synchronization of gas and electricity markets. In recent years, lots of efforts have been made to synchronize the natural gas and electricity markets such as the adjustment of electricity day and gas day [25] and the two markets might be totally synchronized in the future.

B. Distributionally Robust OGPF

In practice, the wind power outputs are difficult to be predicted accurately, while the generation schedule should be made in prior; in real-time dispatch, reserves are committed from eligible units to compensate the discrepancy between generation and demand; reserve capacities are restricted by

$$\begin{aligned} 0 \le r^{+}_{\{\cdot\}t} &\le u_{\{\cdot\}t}\bar{p}_{\{\cdot\}} - p_{\{\cdot\}t}, \\ 0 \le r^{-}_{\{\cdot\}t} &\le p_{\{\cdot\}t} - u_{\{\cdot\}t}\underline{p}_{\{\cdot\}}, \\ \{\cdot\} = \{g,n\}, &\forall n \in \mathcal{N}, \forall g \in \mathcal{G}, \forall t \in \mathcal{T}. \end{aligned} \tag{3}$$

Taking reserve provision into account, ramping limits (1e) and (1f) should be modified as

$$\begin{aligned} p_{\{\cdot\}t} + r^{+}_{\{\cdot\}t} - p_{\{\cdot\},t+1} - r^{-}_{\{\cdot\},t+1} \le \\ u_{\{\cdot\},t+1}P^{-}_{\{\cdot\}} + \left(1 - u_{\{\cdot\},t+1}\right)\bar{p}_{\{\cdot\}}, \\ p_{\{\cdot\},t+1} + r^{+}_{\{\cdot\},t+1} - p_{\{\cdot\}t} - r^{-}_{\{\cdot\}t} \le \\ u_{\{\cdot\}t}P^{+}_{\{\cdot\}} + \left(1 - u_{\{\cdot\}t}\right)\bar{p}_{\{\cdot\}}, \\ \{\cdot\} = \{g,n\}, \forall n \in \mathcal{N}, \forall g \in \mathcal{G}, \forall t \in \mathcal{T}. \end{aligned} \tag{4}$$

In practice, units adjust their outputs according to constant ratios, which is called affine policy [26]. The deployment of reserve can be modeled as

$$\begin{aligned} -r^{-}_{\{\cdot\}t} \le \alpha_{\{\cdot\}t}\textstyle\sum_{w\in\mathcal{W}}(p_{wt} - \tilde{p}_{wt}) \le r^{+}_{\{\cdot\}t}, \\ \{\cdot\} = \{g,n\}, \forall n \in \mathcal{N}, \forall g \in \mathcal{G}, \forall t \in \mathcal{T}, \end{aligned} \tag{5a}$$

$$0 \le \alpha_{\{\cdot\}t} \le 1,\ \{\cdot\} = \{g,n\}, \forall n \in \mathcal{N}, \forall g \in \mathcal{G}, \forall t \in \mathcal{T}, \tag{5b}$$

$$\sum_{g\in\mathcal{G}} \alpha_{gt} + \sum_{n\in\mathcal{N}} \alpha_{nt} = 1,\ \forall t \in \mathcal{T}, \tag{5c}$$

where $\alpha_{\{\cdot\}t}\sum_{w\in\mathcal{W}}(p_{wt} - \tilde{p}_{wt})$ represent incremental output of units and (5a) gives the limits of the real-time adjustments within the reserve offer; (5b) defines the bounds for participation factors; (5c) guarantees the deviations of the wind farms are fully mitigated. In addition, the power flow limits of transmission lines should not be violated with the adjustments of generation outputs, which implies

$$\begin{aligned} \Big|\sum_{g\in\mathcal{G}} \pi_{gl_e}\Big(p_{gt} + \alpha_{gt}\sum_{w\in\mathcal{W}}(p_{wt} - \tilde{p}_{wt})\Big) + \sum_{w\in\mathcal{W}} \pi_{wl_e}\tilde{p}_{wt} + \\ \sum_{n\in\mathcal{N}} \pi_{nl_e}\Big(p_{nt} + \alpha_{nt}\sum_{w\in\mathcal{W}}(p_{wt} - \tilde{p}_{wt})\Big) - \sum_{d_e\in\mathcal{D}_e} \pi_{d_el_e}p_{d_et}\Big| \\ \le p_{le},\ \forall l_e \in \mathcal{L}_e,\ \forall t \in \mathcal{T}. \end{aligned} \tag{6}$$

The fuel consumption of gas-fired units is supplied by the gas system, including the uncertain fuel demands during reserve deployment. The actual fuel demand of gas-fired unit g in period t consists a deterministic part q^{d}_{gt}, which is associated with p_{gt} and known in advance, and an uncertain part q^{u}_{gt}, which depends on the actual utilization of reserve capacity. Fig. 1 gives an illustration of gas supply for q^{u}_{gt}.

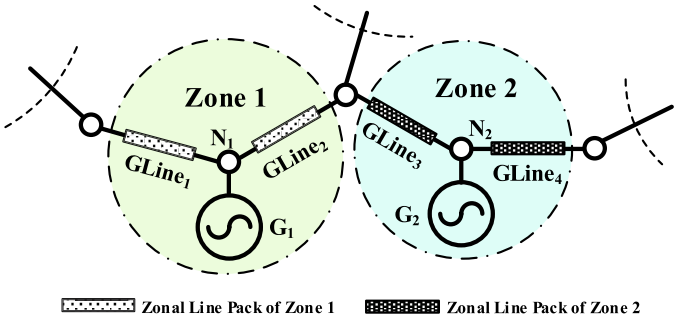

Fig. 1. Illustration of Zonal Line Pack.

In Fig. 1, gas-fired units G_1 and G_2 connect to the gas system through nodes N_1 and N_2, respectively. Then, the uncertain parts of gas demands of G_1 (G_2) are supported by $GLine_1$ and $GLine_2$ ($GLine_3$ and $GLine_4$), considering the relative slow dynamics of the gas system. Zonal line pack is defined as the line packs whose head or tail node connects to gas-fired unit g, and is indexed by g to specify the fuel suppliers. Although line packs provide additional regulation flexibility for gas systems, the total line packs should keep balance periodically, like an electricity storage unit, to maintain sufficient regulation capability for the next cycle. Therefore, the concept of line pack reserve is proposed, which is similar with the electricity reserve, to quantify the impacts of q^{u}_{gt} on the gas system. The relationship between q^{u}_{gt} and committed line pack reserves can be cast as

$$\begin{aligned} -\sum_{l_g\in\Theta_{l_g}(g)} m^{g,-}_{l_gt} \le \alpha_{gt}\sum_{w\in\mathcal{W}} \sigma\left(p_{wt} - \tilde{p}_{wt}\right)/\eta_g \\ \le \sum_{l_g\in\Theta_{l_g}(g)} m^{g,+}_{l_gt}, \forall g \in \mathcal{G},\ \forall t \in \mathcal{T}. \end{aligned} \tag{7}$$

Meanwhile, the committed line pack reserves can not exceed the upper and lower bounds of q^{u}_{gt}, resulting in

$$\sum_{l_g\in\Theta_{l_g}(g)} m^{g,-}_{l_gt} \le \sigma \cdot r^{-}_{gt}/\eta_g,\ \forall g \in \mathcal{G},\ \forall t \in \mathcal{T}, \tag{8a}$$

$$\sum_{l_g\in\Theta_{l_g}(g)} m^{g,+}_{l_gt} \le \sigma \cdot r^{+}_{gt}/\eta_g,\ \forall g \in \mathcal{G},\ \forall t \in \mathcal{T}. \tag{8b}$$

In addition, line packs should always maintain reasonable levels for sustainable utilization, yielding

$$m_{l_gt} + \sum_{t^*=1}^{t}\sum_{g\in\Psi_g(l_g)} m^{g,-}_{l_gt^*} \le \bar{m}_{l_gt},\ \forall l_g \in \mathcal{L}_g,\ \forall t \in \mathcal{T}, \tag{9a}$$

$$\underline{m}_{l_gt} \le m_{l_gt} - \sum_{t^*=1}^{t}\sum_{g\in\Psi_g(l_g)} m^{g,+}_{l_gt^*}, \forall l_g \in \mathcal{L}_g,\ \forall t \in \mathcal{T}, \tag{9b}$$

where $\bar{m}_{l_gt}$ and $\underline{m}_{l_gt}$ are the allowable upper and lower bounds of line packs, respectively. Considering gas system operating

$$\min_{\Lambda}\Bigg\{\sum_{t\in\mathcal{T}}\Big(\sum_{n\in\mathcal{N}}\Big(f_n(p_{nt})+f_n^{+}(r_{nt}^{+})+f_n^{-}(r_{nt}^{-})\Big)+\sum_{e\in\mathcal{E}}Q_{et}q_{et}+\sum_{l_g\in\mathcal{L}_g}\Big(f_{l_g}^{+}(\sum_{g\in\Psi_g(l_g)}m_{l_gt}^{g,+})+f_{l_g}^{-}(\sum_{g\in\Psi_g(l_g)}m_{l_gt}^{g,-})\Big)+$$
$$\max_{\mu\in\mathcal{M}}\mathbb{E}_{\mu}\sum_{t\in\mathcal{T}}\Big[\beta_{d_e}\Big(\sum_{n\in\mathcal{N}}\Big(\alpha_{nt}\sum_{w\in\mathcal{W}}(p_{wt}-\tilde{p}_{wt})-r_{nt}^{+}\Big)^{+}+\sum_{g\in\mathcal{G}}\Big(\alpha_{gt}\sum_{w\in\mathcal{W}}(p_{wt}-\tilde{p}_{wt})-\eta_g\sum_{l_g\in\Theta_{l_g}(g)}m_{l_gt}^{g,+}/\sigma\Big)^{+}\Big)$$
$$+\beta_w\Big(\sum_{n\in\mathcal{N}}\Big(\alpha_{nt}\sum_{w\in\mathcal{W}}(\tilde{p}_{wt}-p_{wt})-r_{nt}^{-}\Big)^{+}+\sum_{g\in\mathcal{G}}\Big(\alpha_{gt}\sum_{w\in\mathcal{W}}(\tilde{p}_{wt}-p_{wt})-\eta_g\sum_{l_g\in\Theta_{l_g}(g)}m_{l_gt}^{g,-}/\sigma\Big)^{+}\Big)$$
$$+\beta_{l_e}\sum_{l_e\in\mathcal{L}_e}\Big(\Big|\sum_{n\in\mathcal{N}}\pi_{nl_e}\Big(p_{nt}+\alpha_{nt}\sum_{w\in\mathcal{W}}\Big(p_{wt}-\tilde{p}_{wt}\Big)\Big)+\sum_{g\in\mathcal{G}}\pi_{gl_e}\Big(p_{gt}+\alpha_{gt}\sum_{w\in\mathcal{W}}(p_{wt}-\tilde{p}_{wt})\Big)$$
$$+\sum_{w\in\mathcal{W}}\pi_{wl_e}\tilde{p}_{wt}-\sum_{d_e\in\mathcal{D}_e}\pi_{d_el_e}p_{d_et}\Big|-p_{l_e}\Big)^{+}\Big]\Bigg\}$$
$$\Lambda=\{p_{gt},p_{nt},r_{gt}^{+},r_{gt}^{-},r_{nt}^{+},r_{nt}^{-},\alpha_{nt},\alpha_{gt},q_{et},q_{l_gt}^{in},q_{l_gt}^{out},q_{l_gt},m_{l_gt},m_{l_gt}^{g,+},m_{l_gt}^{g,-},\bar{m}_{l_gt},\underline{m}_{l_gt},v_{i_gt},v_{l_g^1t}^{l},v_{l_g^1t}^{h}\} \tag{12}$$

security, the allowable bounds of passive pipelines can be calculated by

$$\bar{m}_{l_gt}=\psi_{l_g}\left(v_{l_g^1t}^{h}+\bar{v}_{l_g^2t}\right),\forall l_g\in\mathcal{L}_g/\mathcal{L}_g^c,\forall t\in\mathcal{T}, \tag{10a}$$
$$\underline{m}_{l_gt}=\psi_{l_g}\left(v_{l_g^1t}^{l}+\underline{v}_{l_g^2t}\right),\forall l_g\in\mathcal{L}_g/\mathcal{L}_g^c,\forall t\in\mathcal{T}, \tag{10b}$$
$$\left(q_{l_gt}\right)^2=\phi_{l_g}\left(\left(v_{l_g^1t}^{h}\right)^2-\left(\bar{v}_{l_g^2}\right)^2\right),\forall l_g\in\mathcal{L}_g/\mathcal{L}_g^c,\ \forall t\in\mathcal{T}, \tag{10c}$$
$$\left(q_{l_gt}\right)^2=\phi_{l_g}\left(\left(v_{l_g^1t}^{l}\right)^2-\left(\underline{v}_{l_g^2}\right)^2\right),\forall l_g\in\mathcal{L}_g/\mathcal{L}_g^c,\ \forall t\in\mathcal{T}, \tag{10d}$$

where (10a)-(10b) determine maximum/minimum line pack level from allowable nodal gas pressures; based on pressure bounds $(\underline{v}_{l_g^2},\bar{v}_{l_g^2})$ at the tail node, (10c)-(10d) estimate allowable pressures bounds $(v_{l_g^1t}^{l},v_{l_g^1t}^{h})$ at the head node to ensure the deliverability of gas flow q_{l_gt}. For active pipelines, the maximum and minimum line pack levels can be calculated from

$$\bar{m}_{l_gt}=\psi_{l_g}\left(\bar{v}_{l_g^1}+\bar{v}_{l_g^2}\right),\ \forall l_g\in\mathcal{L}_g^c,\ \forall t\in\mathcal{T}, \tag{11a}$$
$$\underline{m}_{l_gt}=\psi_{l_g}\left(\underline{v}_{l_g^1}+\underline{v}_{l_g^2}\right),\ \forall l_g\in\mathcal{L}_g^c,\ \forall t\in\mathcal{T}, \tag{11b}$$

where subscripts l_g^1 and l_g^2 represent the initial and terminal nodes of an active pipeline, respectively.

As $\tilde{p}_{wt}$ is uncertain, (5a), (6), and (7) may be violated in extreme conditions. The expected constraint violation of (5a), (6), and (7) are penalized in the objective function, which is a common practice in power systems operation [27]. We aim to minimize the objective under the worst-case distribution of the random variables, rendering the following distributionally robust optimization model for OGPF:

$$\begin{aligned}&\text{Objective: }(12)\\&\text{s.t.: }(1b)\text{-}(1d),\ (1g)\text{-}(1k),\ (1m)\text{-}(1o),\ (2)\text{-}(4),\\&\quad(5b)\text{-}(5c),\ (8)\text{-}(11).\end{aligned} \tag{13}$$

In the objective function (12), the first and fourth terms are identical to (1a); the second and third terms are regulation costs for committing upward and downward reserves from non-gas units, respectively, where $f_n^{+}(\cdot)$ and $f_n^{-}(\cdot)$ are convex functions; the fifth and sixth terms are regulation costs for committing upward and downward line pack reserves, respectively, where both $f_{l_g}^{+}(\cdot)$ and $f_{l_g}^{-}(\cdot)$ are convex functions; remaining terms are penalties for load shedding, wind power curtailment and line overload, respectively; and μ is any distribution in the distributional uncertainty set $\mathcal{M}$ that will be specified in Section II-C; $\mathbb{E}$ is the expectation operator; and $(\cdot)^{+}$ is defined as $\max(0,\cdot)$; Λ gathers all the decision variables in problem (13).

Remark 2: Affine policy reserve utilization rule is quite popular in distributionally robust optimization based power system decision-making works, such as [15], [16], [28], [29], as it can offer tractable and equivalent reformulations under quite a few distributional uncertainty sets, including moment based ones and Wasserstein distance based ones. Meanwhile, from application perspective, affine policy is employed in many practical decision-making frameworks of electricity industry due to its simplicity, such as auto generation control (AGC) [30]. It should be pointed out that the affine policy reserve utilization rule would lead to more conservative results compared with the fully dispatchable reserve utilization rule in [31]. A practical and computational efficient distributionally robust model for the OGPF problem using fully dispatchable reserve utilization rule would be one of our future research directions.

Remark 3: In accordance with [16], [27], [28], the electricity reserve utilization costs are not included in (12). Nevertheless, they can be easily incorporated into the proposed DROGPF model by replacing the terms in the second and

third lines of (12) inside the brackets with

$$\begin{aligned}
&\sum_{n\in\mathcal{N}}(\beta_{d_e}-\beta_{nt}^{+})\Big(\alpha_{nt}\sum_{w\in\mathcal{W}}(p_{wt}-\tilde{p}_{wt})-r_{nt}^{+}\Big)^{+}\\
&+\sum_{g\in\mathcal{G}}(\beta_{d_e}-\beta_{gt}^{+})\Big(\alpha_{gt}\sum_{w\in\mathcal{W}}(p_{wt}-\tilde{p}_{wt})-\eta_g\sum_{l_g\in\Theta_{l_g}(g)}\frac{m_{l_gt}^{g,+}}{\sigma}\Big)^{+}\\
&+\sum_{n\in\mathcal{N}}(\beta_{w}-\beta_{nt}^{-})\Big(\alpha_{nt}\sum_{w\in\mathcal{W}}(\tilde{p}_{wt}-p_{wt})-r_{nt}^{-}\Big)^{+}\\
&+\sum_{g\in\mathcal{G}}(\beta_{w}-\beta_{gt}^{-})\Big(\alpha_{gt}\sum_{w\in\mathcal{W}}(\tilde{p}_{wt}-p_{wt})-\eta_g\sum_{l_g\in\Theta_{l_g}(g)}\frac{m_{l_gt}^{g,-}}{\sigma}\Big)^{+}\\
&+\sum_{n\in\mathcal{N}}\sum_{w\in\mathcal{W}}\alpha_{nt}\Big(\beta_{nt}^{+}(p_{wt}-\tilde{p}_{wt})^{+}+\beta_{nt}^{-}(\tilde{p}_{wt}-p_{wt})^{+}\Big)\\
&+\sum_{g\in\mathcal{G}}\sum_{w\in\mathcal{W}}\alpha_{gt}\Big(\beta_{gt}^{+}(p_{wt}-\tilde{p}_{wt})^{+}+\beta_{gt}^{-}(\tilde{p}_{wt}-p_{wt})^{+}\Big),
\end{aligned}\tag{14}$$

where $\beta_{nt}^{+}(\beta_{nt}^{-})$ and $\beta_{gt}^{+}(\beta_{gt}^{-})$ are the upward (downward) reserve utilization cost coefficients of non-gas and gas-fired generators, respectively. In (14), the last two lines describe the reserve utilization costs of non-gas and gas-fired generators, respectively.

C. Construction of the Distributional Uncertainty Set

Before tackling the proposed model (13), it is crucial to specify a meaningful and tractable distributional uncertainty set. Let $\nu := \frac{1}{S}\sum_{s=1}^{S}\delta_{\hat{\boldsymbol{\xi}}^s}$ be the empirical distribution, where $\hat{\boldsymbol{\xi}}^s, s=1,\ldots,S$ are samples and $\delta_{\hat{\boldsymbol{\xi}}^s}$ represents the Dirac measure on $\hat{\boldsymbol{\xi}}^s$. To restrict the statistical distance between any candidate distribution $\mu\in\mathcal{M}$ and the empirical distribution ν, we define

$$\mathcal{M} := \Big\{\mu\in\mathcal{P}:\mathbb{D}(\mu,\nu)\le\theta\Big\},$$

where θ is a positive parameter, and $\mathbb{D}(\mu,\nu)$ is the Wasserstein distance between two distributions μ and ν, which is given by

$$\mathbb{D}(\mu,\nu) := \min_{\gamma}\Big\{\int_{\mathbb{R}^W\times\mathbb{R}^W}\|\boldsymbol{\xi}-\boldsymbol{\zeta}\|\,\gamma\Big(\mathrm{d}\boldsymbol{\xi},\mathrm{d}\boldsymbol{\zeta}\Big)\Big\},\tag{15}$$

where γ is a joint distribution on $\mathbb{R}^W\times\mathbb{R}^W$ with marginals μ,ν; $\boldsymbol{\xi},\boldsymbol{\zeta}$ are the integral variables; $\|\cdot\|$ stands for Euclidean norm. Thus $\mathcal{M}$ contains all probability distributions whose Wasserstein distances to the empirical distribution are no greater than θ.

Intuitively, the joint distribution γ on the right-hand side of (15) above can be viewed as a transportation plan which transports probability mass from ν to μ. Thus, the Wasserstein metric between two distributions equals the cheapest cost (measured in some norm $\|\cdot\|$) of transporting probability mass from one distribution to the other. Wasserstein metric has recently become popular in machine learning as a way to measuring the distance between probability distributions, and has been applied to a variety of areas including computer vision, generative adversarial networks, and distributionally robust optimization [32].

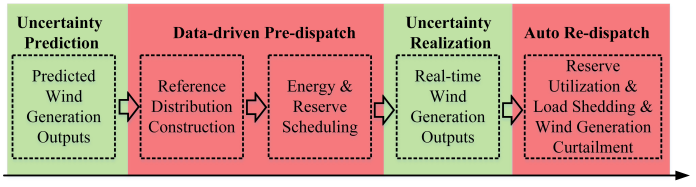

Fig. 2. Decision process illustration.

Wasserstein distance is well suited for hedging against the perturbation of data values and has good out-of-sample performance [17], [33]. Since $\mathcal{M}$ is comprised of infinitely many distributions, the proposed (13) model is not immediately computationally tractable, and we will provide a tractable formulation in the next section.

Remark 4: In this work, a multi-period OGPF model is tackled. Therefore, it could be applied to either day-ahead scheduling or real-time lookahead dispatch.

In practice, the real-time accommodated wind generation could be lower than its actual value, which depends on the deliverable downward reserves r_{gt}^{-}, r_{nt}^{-}. If total amount of deliverable downward reserves is insufficient, wind generation curtailment would occur. By this means, the scheduled wind generation outputs become decision variables. Meanwhile, wind generation curtailment is penalized in the objective function, which indicates the operator of the integrated electricity-gas system (IEGS) could weigh the benefits of wind generation accommodation and the costs of additional electricity reserve for wind generation uncertainty mitigation, and then determine the accommodated amount of wind generation.

An illustration of the decision process is shown as Fig. 2. It can be observed the decision-making of the IEGS operator contains two stages, which are the data-driven pre-dispatch and the auto re-dispatch, respectively. In the first stage, the IEGS operator constructs the reference distribution of wind generation outputs according to their predicted curves as well as qualified historical data, and then determines the energy and reserve schedule. In the second stage, reserves are automatically utilized based on their participation factors determined in the first stage as well as the total wind generation outputs deviation. It should be noted that the deployed reserves might be insufficient in some extreme scenarios, resulting in either load shedding or wind generation curtailment.

Remark 5: In fact, distributional uncertainty sets (DUSs) reported by existing power system distributionally robust decision-making works can be divided into three categories, which are

1) Moment-based DUSs, among which the first- and second-order moment conditions are the most common. In [15], [16], [28], the sets of all probability distributions are specified by the given mean and covariance of the random variables, where semidefinite programmings (SDPs) are tackled after model reformulations and the corresponding computational burden is relatively high. [34] and [14] drop the covariance constraint and add other first-order constraints in their DUSs, leading to

linear programming (LP) reformulations of the distributionally robust models, which significantly reduces the computational burden.

2) Kullback-Leibler (KL) divergence-based DUSs. In [35], the KL divergence-based DUS is equivalently transformed into the respective classical chance constraints under the nominal distribution but with a rescaled violation probability.
3) Wasserstein distance based DUSs. [29] adopts the Wasserstein metric based DUS and its tractable reformulation is also an LP. It should be noted that though the DUS in [29] is similar to the one in our work, they are completely different works and the major differences are: i. the model in [29] is a chance-constrained programming (CCP) and the aftermath of constraint violation is not considered; ii. our work minimizes the violation of random variable involved constraints. The aforementioned differences would result in totally different tractable reformulation procedures of the distributionally robust models.

Among the aforementioned three types of DUSs, the moment-based ones require the smallest amount of information of the uncertainties, yet their conservativeness are relatively high; the KL divergence based ones are much less conservative, however, they must assign positive probability mass to each training sample and their out-of-sample performances cannot be guaranteed [36]. The Wasserstein distance based DUSs overcome the deficiencies of those two approaches, where the qualified samples are adopted to construct the reference distribution without assigning probability weights, the parameters are chosen based on modern measure concentration, and their tractable reformulations are second-order cone or linear programmings [36]. Therefore, the proposed Wasserstein metric based DUS is more suitable for the DROGPF problem from mathematical, computational and practical perspectives.

III. Solution Methodology

Note that the proposed DROGPF model (13) is not readily solvable by commercial solvers, due to the nonconvexities in the constraints, i.e., the Weymouth equations (2a), (10c), and (10d), which are quadratic equalities, and intractable terms in the objective function, namely, the last three lines of (12), which describes the maximization of the operation loss expectation under the worst-case distribution.

In what follows, a convexification method for the Weymouth equations is introduced, and then a tractable reformulation of the proposed DROGPF objective function is derived, after which a convex and tractable approximation of problem (13) can be obtained. To mitigate the solution infeasibility issue caused by the constraint convexification treatment, a sequential convex programming based algorithm is devised to enhance the solution feasibility of the convexified counterpart of problem (13) with respect to the original problem. The overall solution procedure is shown in Fig. 3.

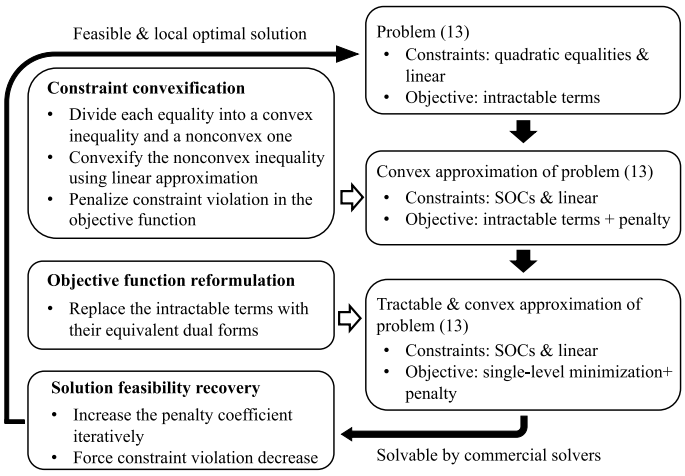

Fig. 3. The convex optimization based solution procedure.

A. Convexification of the DROGPF Constraints

In the proposed DROGPF, all constraints are linear except for Weymouth equations in (2a), (10c), and (10d), in form of

$$a^2 = b_1^2 - b_2^2, \tag{16}$$

which can be cast as opposite inequalities as

$$a^2 \le b_1^2 - b_2^2, \tag{17a}$$
$$b_1^2 \le a^2 + b_2^2, \tag{17b}$$

where (17a) is an SOC whose canonical form is given by

$$\left\| \begin{array}{c} a \\ b_2 \end{array} \right\|_2 \le b_1. \tag{18}$$

Given a vector $[a^{(\varrho)}\ b_2^{(\varrho)}]^\top$, the linear approximation of the righthand side terms of (17b) is

$$a^2 + b_2^2 \approx 2a^{(\varrho)}a - (a^{(\varrho)})^2 + 2b_2^{(\varrho)}b_2 - (b_2^{(\varrho)})^2. \tag{19}$$

After replacing the right-hand side terms of (17b) by (19) and adding a positive slack variable $\zeta^{(\varrho)}$, (17b) can be approximated by a rotated quadratic cone as [37]

$$b_1^2 \le 2a^{(\varrho)}a - (a^{(\varrho)})^2 + 2b_2^{(\varrho)}b_2 - (b_2^{(\varrho)})^2 + \zeta^{(\varrho)}. \tag{20}$$

For the sake of exposition, the compact form of the proposed DROGPF model with convexified Weymouth equations is given in a compact form

$$\min_{\boldsymbol{x},\boldsymbol{\zeta}\ge\mathbf{0}} \quad \boldsymbol{f}(\boldsymbol{x}) + \tau\mathbf{1}^\top\boldsymbol{\zeta} + \max_{\mu\in\mathcal{M}} \mathbb{E}_\mu[\Theta(\boldsymbol{x},\boldsymbol{\xi})] \tag{21a}$$
$$\text{s.t.} \quad \boldsymbol{A}\boldsymbol{x} \le \boldsymbol{b} \tag{21b}$$
$$\left\|\tilde{\boldsymbol{E}}^z_{l_gt}\boldsymbol{x} + \tilde{\boldsymbol{F}}^z_{l_gt}\boldsymbol{\zeta} + \tilde{\boldsymbol{g}}^z_{l_gt}\right\|_2 \le (\tilde{\boldsymbol{m}}^z_{l_gt})^\top\boldsymbol{x} + (\tilde{\boldsymbol{n}}^z_{l_gt})^\top\boldsymbol{\zeta} + \tilde{o}^z_{l_gt}, \tag{21c}$$
$$\left\|\boldsymbol{G}^z_{l_gt}\boldsymbol{x} + \boldsymbol{h}^z_{l_gt}\right\|_2 \le (\boldsymbol{c}^z_{l_gt})^\top\boldsymbol{x} + \rho^z_{l_gt}, \tag{21d}$$
$$\forall\ l_g \in \mathcal{L}_g/\mathcal{L}_g^c,\ \forall\ t\in\mathcal{T},\ z=\{1,2,3\}$$

where $\boldsymbol{x}$ is the vector of decision variables of problem (13); $\boldsymbol{\zeta}$ is the vector of slack variables; $\boldsymbol{\xi}$ is the vector of random variables; $\boldsymbol{A}$ and $\boldsymbol{b}$ are coefficients for the linear constraints,

which can be derived from constraints of problem (13) except (2a), (10c), and (10d); $\tilde{\boldsymbol{E}}^z_{l_g t}$, $\tilde{\boldsymbol{F}}^z_{l_g t}$, $\tilde{\boldsymbol{g}}^z_{l_g t}$, $\tilde{\boldsymbol{m}}^z_{l_g t}$, $\tilde{\boldsymbol{n}}^z_{l_g t}$, $\tilde{o}^z_{l_g t}$, $\boldsymbol{G}^z_{l_g t}$, $\boldsymbol{h}^z_{l_g t}$, $\boldsymbol{c}^z_{l_g t}$, $\rho^z_{l_g t}$ are coefficients for the SOC constraints generated during Weymouth equation convexification, and can be obtained from (2a), (10c), and (10d); $\boldsymbol{f}(\cdot)$ expresses the sum of the first row in (12); τ is the penalty coefficient and $\tau \mathbf{1}^\top \boldsymbol{\zeta}$ represents the violation penalty of Weymouth equations; and

$$\Theta(\boldsymbol{x}, \boldsymbol{\xi}) = \max_{1 \le k \le K} \ \boldsymbol{a}_k(\boldsymbol{x})^\top \boldsymbol{\xi} + b_k(\boldsymbol{x}) \tag{22}$$

expresses the piecewise linear convex function of $\boldsymbol{\xi}$ inside the expectation $\mathbb{E}_\mu$ in (12), where k is the index for the piecewise linear segment in (22), $K = 4^{(G+N)T} \times 3^{L_e T}$, $\boldsymbol{a}_k(\boldsymbol{x}), b_k(\boldsymbol{x})$ are coefficients that can be derived from (12) and their detailed expressions are provided in Appendix A.

In problem (21), the coefficients with tildes are not constant. Specifically, they are linear functions of the initial values of $q_{l_g t}, v_{i_g t}$, and can be calculated in advance.

B. Tractable Reformulation of the DROGPF Objective

According to Corollary 2 in [17], (21) can be replaced by its dual as follows.

$$\min_{\substack{\boldsymbol{x},\boldsymbol{y},\boldsymbol{\zeta} \ge \mathbf{0} \\ \lambda \ge 0}} \ \boldsymbol{f}(\boldsymbol{x}) + \tau \mathbf{1}^\top \boldsymbol{\zeta} + \lambda\theta + \frac{1}{S}\sum_{s=1}^{S} y_s \tag{23a}$$

$$s.t.\ y_s \ge \boldsymbol{a}_k(\boldsymbol{x})^\top \hat{\boldsymbol{\xi}}^s + b_k(\boldsymbol{x}),\ \forall 1 \le k \le K,\ s \in \mathcal{S}, \tag{23b}$$

$$\begin{aligned} &\lambda \ge \max\Big\{ \|\boldsymbol{a}^{gt}_{j^{gt}_{d_e}}(\boldsymbol{x})\|, \|\boldsymbol{a}^{gt}_{j^{gt}_{w}}(\boldsymbol{x})\|, \|\boldsymbol{a}^{nt}_{j^{nt}_{d_e}}(\boldsymbol{x})\|, \\ &\|\boldsymbol{a}^{nt}_{j^{nt}_{w}}(\boldsymbol{x})\|, \|\boldsymbol{a}^{l_e t}_{j^{t}_{l_e}}(\boldsymbol{x})\| \Big\}, \forall t \in \mathcal{T}, g \in \mathcal{G}, n \in \mathcal{N}, \\ &l_e \in \mathcal{L}_e,\ j^{gt}_{d_e}, j^{gt}_{w}, j^{nt}_{d_e}, j^{nt}_{w} \in \{1,2\}, j^{t}_{l_e} \in \{1,2,3\} \\ &(21b),\ (21c),\ (21d). \end{aligned} \tag{23c}$$

In (23), $y_s, s = 1, \ldots, S$ and λ are auxiliary variables; $\boldsymbol{a}^{gt}_{j^{gt}_{d_e}}(\boldsymbol{x})$, $\boldsymbol{a}^{gt}_{j^{gt}_{w}}(\boldsymbol{x})$, $\boldsymbol{a}^{nt}_{j^{nt}_{d_e}}(\boldsymbol{x})$, $\boldsymbol{a}^{nt}_{j^{nt}_{w}}(\boldsymbol{x})$, $\boldsymbol{a}^{l_e t}_{j^{t}_{l_e}}(\boldsymbol{x})$ are coefficients and their expressions can be found in Appendix A. In (23), the objective function (23a) is convex, constraints (23b) is linear and (23c) is equivalent to SOCs. Evidently, (23) suggests an SOCP, which can be efficiently solved.

There are $4^{(G+N)T} \times 3^{L_e T} \times S$ linear inequalities in (23b); nevertheless, after substituting (23b) and y_s in (23a) by their equivalent forms, respectively, the number of constraints in (23b) can be reduced to $(4G + 4N + 3L_e) \times S \times T$. Details are provided in Appendix B.

C. Solution Feasibility Recovery

To enhance the solution feasibility of problem (23) with respect to problem (13), a sequential SOCP algorithm is developed. The flowchart is summarized in Algorithm 1, whose convergence proof can be found in [38]. By properly selecting the penalty parameter, a local optimal solution of (13) can be recovered once Algorithm 1 converges. However, different from existing local algorithm for nonlinear programs, Algorithm 1 starts from a convex relaxation model, and makes no reference to an initial point. For the same reason, the final solution is very likely to be the global one of problem (13).

Algorithm 1 S-SOCP for problem (23)

1: Initialize the penalty parameters $\tau^{(0)}, \tau_{\max}, \kappa > 1$ and convergence parameters ϵ, ε. Set the iteration index $\varrho = 0$. Solve the following dual reformulation of the relaxed OGPF problem

$$\begin{aligned} Obj = \min_{\boldsymbol{x},\boldsymbol{y},\lambda} \ & \boldsymbol{f}(\boldsymbol{x}) + \lambda\theta + \frac{1}{S}\sum_{s=1}^{S} y_s \\ s.t.\ \ & \lambda \ge 0,\ (21b),\ (21d). \end{aligned} \tag{24}$$

The optimal solutions (values) are $\boldsymbol{x}^{(0)}$,$\boldsymbol{y}^{(0)}$,$\lambda^{(0)}$ ($Obj^{(0)}$).

2: Update coefficients of the convexified Weymouth equation in (21c) at $\boldsymbol{x}^{(\varrho)}$. Solve the following SOCP

$$\begin{aligned} \min_{\boldsymbol{x},\boldsymbol{y},\boldsymbol{\zeta},\lambda} \ & \boldsymbol{f}(\boldsymbol{x}) + \tau^{(\varrho)} \mathbf{1}^\top \boldsymbol{\zeta} + \lambda\theta + \frac{1}{S}\sum_{s=1}^{S} y_s \\ \text{s.t.}\ \ & (21b), (21c), (21d),\ \boldsymbol{\zeta} \ge \mathbf{0},\ \lambda \ge 0 \end{aligned} \tag{25}$$

$\varrho \leftarrow \varrho + 1$. The optimal solutions are $\boldsymbol{x}^{(\varrho)}$,$\boldsymbol{y}^{(\varrho)}$,$\lambda^{(\varrho)}$,$\boldsymbol{\zeta}^{(\varrho)}$, with the optimal value of $Obj^{(\varrho)}$.

3: If (26) holds, then terminate and report the optimal solution; otherwise, update $\tau^{(\varrho)} = \min(\kappa\tau^{(\varrho-1)}, \tau_{\max})$, and go to Step 2.

$$\begin{aligned} &|Obj^{(\varrho)} - Obj^{(\varrho-1)}| \le \epsilon \\ &\zeta^{z,(\varrho)}_{l_g t} \le \varepsilon \left(q^{(\varrho)}_{l_g t}\right)^2, \forall l_g \in \mathcal{L}_g / \mathcal{L}^c_g,\ \forall t \in \mathcal{T},\ z = \{1,2,3\}. \end{aligned} \tag{26}$$

IV. Illustrative Example

In this section, we present numerical experiments on a test system to validate the effectiveness of the proposed methods. Experiments are carried out on a laptop with Intel ® Xeon® 3.7 GHz CPU and 64 GB memory. The proposed algorithms are coded in MATLAB with YALMIP toolbox. SOCPs are solved by Gurobi 7.5. Parameters of the solver are default without particular mention.

A. System Configuration

Fig. 4 depicts the topology of the connected infrastructure, where the power grid possesses 2 gas-fired units, 1 non-gas unit, 2 wind farms, 6 transmission lines and 3 loads; the gas system consists of 2 gas wells, 4 passive pipelines, 2 compressors and 3 loads. In Fig. 4, we use B, G, W, PL, PLine with subscripts to denote electricity buses, units, wind farms, electricity loads, and transmission lines, respectively, and N, C, GL, GW, GLine with subscripts to denote gas nodes, compressors, gas loads, gas wells, and gas passive pipelines, respectively. Specially, the gas fuels of G_1 and G_2 come from N_4 and N_1, respectively. The hourly electricity, gas demands, and total outputs of wind farms are presented in Fig. 5. Complete data of the system can be found in [39]. Set the generation costs function $f_n(\cdot)$ and the reserve costs functions $f^+_n(\cdot)$, $f^-_n(\cdot)$, $f^+_{l_g}(\cdot)$, $f^-_{l_g}(\cdot)$ as quadratic and linear functions, respectively, and cost coefficients values can be

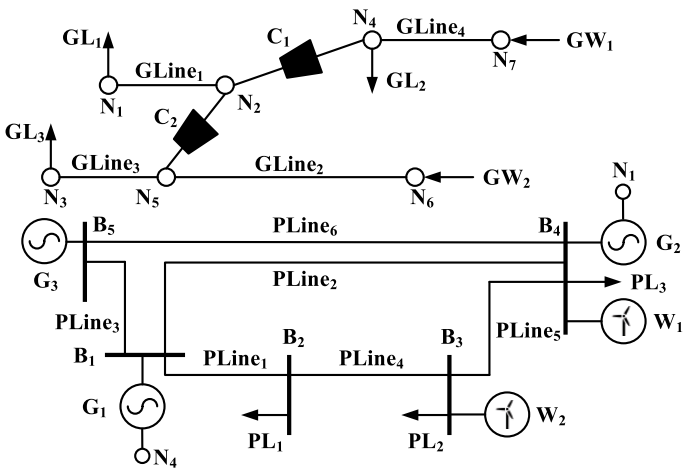

Fig. 4. Topology of the Power5Gas7 system.

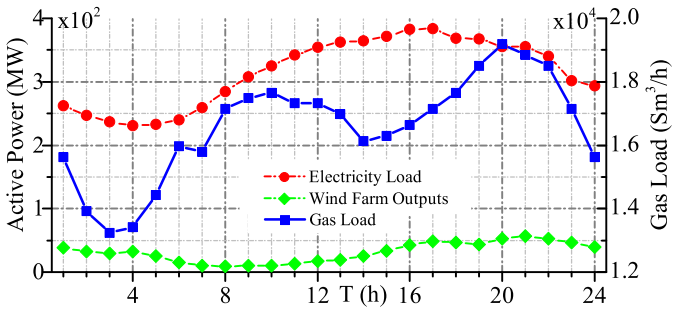

Fig. 5. Wind generation and energy demands of the Power5Gas7 system.

found in [39]. Hereinafter, this system is referred to as the Power5Gas7 system.

B. Sample Generation and Parameter Tuning

We assume $\boldsymbol{\xi}$ follows a multivariate Gaussian distribution, where the mean values of $\boldsymbol{\xi}$ can be found in [39] and the standard deviation of each entry of $\boldsymbol{\xi}$ equals its mean multiplying a scalar randomly chosen from $[0.5, 1]$. To guarantee the validness of the samples, a sample validity checking procedure is developed and executed during sample generation. Specifically, valid samples should satisfy

$$0 \le \hat{p}^s_{wt} \le \bar{p}_w, \ \forall w \in \mathcal{W}, \ t \in \mathcal{T}, \ s \in \mathcal{S}, \tag{27}$$

where $\hat{p}^s_{wt}$ is the outputs of wind farm w in sample $\hat{\boldsymbol{\xi}}^s$; $\bar{p}_w$ is the installed capacity of wind farm w.

The Wasserstein radius θ is selected using hold-out cross validation method, whose detailed procedure is as follows.

Step 1: Divide the sample dataset $\mathcal{S}$, into a training dataset, denoted as $\mathcal{S}_{\rm t}$, which contains 70% samples of $\mathcal{S}$, and a validation dataset, denoted as $\mathcal{S}_{\rm v}$, including the remaining 30% of $\mathcal{S}$. Set $\theta_0 = 0$, $\Delta\theta = 0.01$, $\theta_{\max} = 0.1$, and $\theta = \theta_0$.

Step 2: Solve problem (21), which contains a series of SOCPs, with $\mathcal{S}_{\rm v}$, and record $\boldsymbol{x}$, $\boldsymbol{f}(\boldsymbol{x})$.

Step 3: Parameterize the decision variables in (28), namely α_{gt}, α_{nt}, p_{gt}, p_{nt}, r^+_{nt}, r^-_{nt}, r^+_{gt}, r^-_{gt}, $m^{g,+}_{l_g t}$, $m^{g,-}_{l_g t}$, with $\boldsymbol{x}$ of Step 2, and calculate $R(\boldsymbol{x})$ according to (28), which is the out-of-sample performance of $\boldsymbol{x}$ with the validation dataset $\mathcal{S}_{\rm v}$.

$$\begin{aligned}
R(\boldsymbol{x}) = \sum_{s\in\mathcal{S}_{\rm v}} \Bigg\{ \sum_{t\in\mathcal{T}} \Bigg[& \beta_{d_e} \Bigg(\sum_{n\in\mathcal{N}} \Big(\alpha_{nt} \sum_{w\in\mathcal{W}} (p_{wt} - \hat{p}^s_{wt}) - r^+_{nt} \Big)^+ \\
& + \sum_{g\in\mathcal{G}} \Big(\alpha_{gt} \sum_{w\in\mathcal{W}} (p_{wt} - \hat{p}^s_{wt}) - \eta_g \sum_{l_g\in\Theta_{l_g}(g)} m^{g,+}_{l_g t}/\sigma \Big)^+ \Bigg) \\
& + \beta_w \Bigg(\sum_{n\in\mathcal{N}} \Big(\alpha_{nt} \sum_{w\in\mathcal{W}} (\hat{p}^s_{wt} - p_{wt}) - r^-_{nt} \Big)^+ \\
& + \sum_{g\in\mathcal{G}} \Big(\alpha_{gt} \sum_{w\in\mathcal{W}} (\hat{p}^s_{wt} - p_{wt}) - \eta_g \sum_{l_g\in\Theta_{l_g}(g)} m^{g,-}_{l_g t}/\sigma \Big)^+ \Bigg) \\
& + \beta_{l_e} \sum_{l_e\in\mathcal{L}_e} \Bigg(\Big| \sum_{n\in\mathcal{N}} \pi_{nl_e} \Big(p_{nt} + \alpha_{nt} \sum_{w\in\mathcal{W}} \Big(p_{wt} - \hat{p}^s_{wt} \Big) \Big) \\
& + \sum_{g\in\mathcal{G}} \pi_{gl_e} \Big(p_{gt} + \alpha_{gt} \sum_{w\in\mathcal{W}} (p_{wt} - \hat{p}^s_{wt}) \Big) \\
& + \sum_{w\in\mathcal{W}} \pi_{wl_e} \hat{p}^s_{wt} - \sum_{d_e\in\mathcal{D}_e} \pi_{d_e l_e} p_{d_e t} \Big| - p_{l_e} \Bigg)^+ \Bigg] \Bigg\}
\end{aligned} \tag{28}$$

Step 4: If $\theta < \theta_{\max}$, set $\theta = \theta + \Delta\theta$ and go to Step 2; otherwise, terminate and select θ with the minimum $\boldsymbol{f}(\boldsymbol{x}) + R(\boldsymbol{x})$ as the best tuning value.

With the optimal θ, we resolve problem (23) using all S samples and obtain the optimal solution. Then, the out-of-sample performances of the proposed DROGPF model is examined using an independent testing dataset consists of 10^4 samples.

C. Results

According to Section II.C, the empirical distribution μ is formed by historical samples. However, it should be noted that the candidate sample set for μ only consists a relatively small part of all the historical data, whose meteorological conditions are similar with the ones of the current decision-making stage. Considering the relatively high dimensionality of the random variable vector, which consists the outputs of all the wind farms, there won't be too many available samples in practical applications. Therefore, we assume that the decision maker has limited data on the random variable $\boldsymbol{\xi}$, and use a small sample set with $S = 20$, which is also adopted by [16]. The simulations are repeated by 50 times. The parameters of Algorithm 1 are selected as $\tau^{(0)} = 0.1$, $\tau_{\max} = 10000$, $\kappa = 2$, $\epsilon = 0.001$, $\varepsilon = 0.001$, and $\rho_{\max} = 100$.

1) Comparison with Sample Average Approximation: In the sequel, detailed comparisons are made between the aforementioned approaches, i.e., the proposed distributionally robust model and sample average approximation (SAA) [1], for the

[1]The mathematical formulation of SAA and the proposed DROGPF models are almost the same except that the proposed DROGPF model calculates the expectation of penalized constraint violation under the worst-case distribution μ of random variables, while SAA minimizes the expectation of penalties under empirical distribution ν, which is formed by the samples. Therefore, the SAA formulation also deals with a relaxed counterpart of the original problem, where the expectation of the constraint violations are penalized in the objective function.

TABLE I
COMPARISON OF THE PROPOSED DROGPF MODEL AND SAA FOR THE POWER5GAS7 SYSTEM.

	Average performance			Penalty decrement rate (%)			OP improvement rate (%)		
	OP ($)	DC ($)	Penalty ($)	Average	Best	Worst	Average	Best	Worst
DROGPF	1.586×10^5	1.384×10^5	2.023×10^4	62.37	45.81	10.20	1.546	2.288	0.508
SAA	1.611×10^5	1.248×10^5	3.733×10^4	-	-	-	-	-	-

data-driven OGPF problem. Results are shown in Table I, where column 2 to column 4 describe the average performances of the proposed DROGPF model and SAA of 50 simulation tests, with OP and DC representing out-of-sample performances (dispatch costs plus operational risk under the testing dataset) and dispatch costs (sum of first six terms in (12)), respectively, and column 5 to column 7 summarize the mean as well as upper and lower bounds of relative OP improvement rate of the 50 simulation tests with SAA being the benchmark approach. Specifically, OP equals the sum of DC and penalty for each row in Table I.

From Table I, the average OP of SAA is 1.546% higher than the proposed DROGPF model, as SAA only accounts for the designated distribution (the empirical distribution) generated from S samples, so the result is sensitive to the perturbation in the true distribution of uncertain data. The dispatch costs of SAA and the proposed DROGPF model reflect the differences of their out-of-sample performances. From Table I, though the average dispatch costs of the proposed DROGPF model are 10.91% larger than SAA, indicating the dispatch strategy is more conservative, such as committing more reserves as well as preserving more capacity for heavily loaded transmission lines, its average penalty has a 62.37% decrement compared with SAA, resulting in the 1.546% improvement in out-of-sample performance in return. Among the 50 simulation tests, the OP of the proposed DROGPF is always better than SAA, and the best and the worst improvement rates are 2.288% and 0.508%, respectively, indicating the effectiveness of the proposed DROGPF model.

Specifically, one simulation is selected from the repeated 50 simulation with $S = 20$, and its distributions of the total operational loss as well as the penalized electricity load shedding, wind curtailment, and transmission line overload with 10,000 test samples are demonstrated in Fig. 6. In Fig. 6(a), the 10^4 scenarios are sorted and renumbered according to their operational loss performances with SAA and the proposed DROGPF model, respectively, which means the scenarios with the same index in SAA and DROGPF sorting system might not be the same. And the scenario indices in Fig. 6(b) - 6(d) are the same as Fig. 6(a). It can be observed that the operational losses of SAA are much higher than the proposed DROGPF model, which are mainly caused by the load shedding penalty differences, as shown in Fig. 6(b).

2) Convergence Performance: The sequence of objective value and maximum relative constraint violation (MRCV), which is defined as the positive slack variable divide the corresponding left-hand term of the unrelaxed constraint, generated

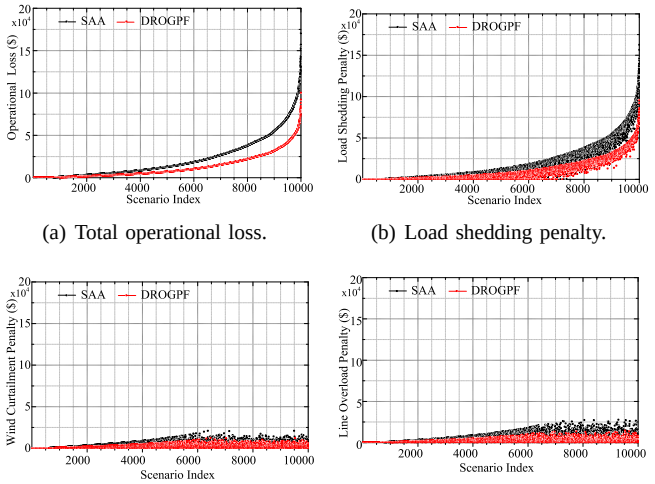

(a) Total operational loss. (b) Load shedding penalty.

(c) Wind curtailment penalty. (d) Line overload penalty.

Fig. 6. Operational loss of the 10^4 test samples from one simulation.

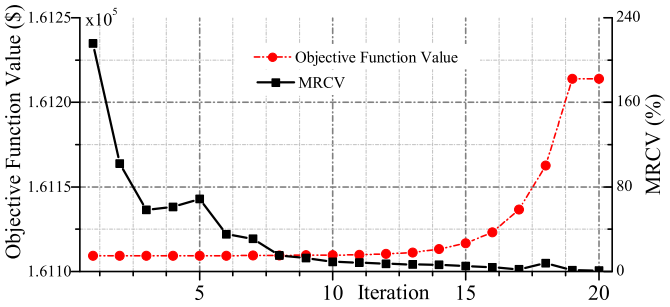

Fig. 7. Objective value and MRCV during iterations of one simulation.

in Algorithm 1 of one simulation are plotted in Fig. 7. The constraint is identified as satisfied if MRCV is below a given threshold, which is 0.01% in this case.

From Fig. 7, Algorithm 1 converges in 20 iterations, and it can be observed that the MRCV at the 1st iteration is 215.6%, indicating the gas system would suffer over-high or over-low pressure at the solution obtained from the relaxed OGPF model, in which non-convex part in form of (17b) in Weymouth equation is neglected. Along with the execution of the algorithm, the MRCV gradually decreases and meets the threshold at the 20th iteration. Meanwhile, the objective function value at the 20th iteration has a 0.265% increment compared with the relaxed model, demonstrating the necessity of the proposed solution tightness enhancement procedure.

3) Impacts of Nodal Pressure Limits: According to (10) and (11), the available amount of line pack reserve depends

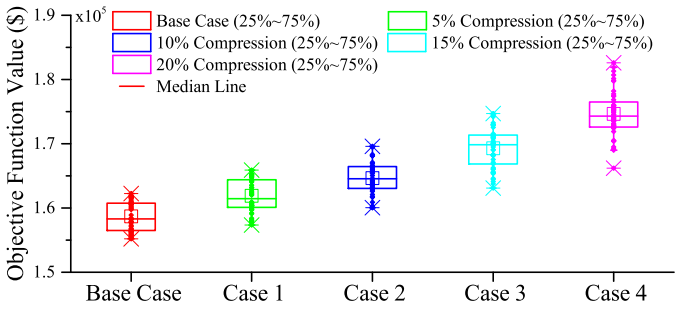

Fig. 8. Simulation results with different gas nodal pressure intervals.

TABLE II
COMPARISON OF THE PROPOSED DROGPF MODEL AND SAA FOR THE POWER5GAS7 SYSTEM WITH $S = 100$ AND $S = 1000$.

		Average OP ($)	OP improvement rate (%)		
			Average	Best	Worst
$S = 100$	DROGPF	1.5749×10^5	1.120	1.764	0.327
	SAA	1.5927×10^5	-	-	-
$S = 1000$	DROGPF	1.5738×10^5	0.300	0.471	0.223
	SAA	1.5785×10^5	-	-	-

on the lower and upper bounds of line pack, which are largely influenced by the gas pressure limits. Therefore, the economic impact of gas pressure limits on the distributionally robust dispatch strategy are analyzed to provide decision support for the determination of proper nodal pressure limits. Specifically, we compress the allowable pressure intervals of gas nodes symmetrically, e.g., $\varsigma\%$ compression means the upper and lower pressure limits of gas nodes are modified as

$$\bar{v}_{i_g}^{(\varsigma)} = \bar{v}_{i_g} - \varsigma\% \times (\bar{v}_{i_g} - \underline{v}_{i_g}),\ \forall i_g \in \mathcal{I}_g, \tag{29a}$$

$$\underline{v}_{i_g}^{(\varsigma)} = \underline{v}_{i_g} + \varsigma\% \times (\bar{v}_{i_g} - \underline{v}_{i_g}),\ \forall i_g \in \mathcal{I}_g. \tag{29b}$$

50 repeated simulations are executed for 5%, 10%, 15%, and 20% compression of allowable pressure interval, respectively; the training, validation, and testing datasets for the five cases remain unchanged. Optimal values and out-of-sample performances are compared with the base case simulations, as shown in Fig. 8.

In the test system, reserves offered by non-gas units are more expensive than line pack reserves considering unit transformation and energy conversion efficiency. On this account, when the allowable nodal pressure intervals become narrower, the power system has to commit more reserves from non-gas units as the line pack reserves, the fuel of gas-fired units during regulation, might be insufficient, indicating the integrated energy system may suffer from higher dispatch costs, or worse, larger operational risk due to the lack of reserve capacities. In Fig. 8, it can be observed that the out-of-sample performances increase as the allowable nodal pressure intervals become narrower, which confirms the previous inference.

4) Impacts of Dataset Size: In the sequel, the proposed models and methods are tested on larger sample sets, where $S = 100$ and $S = 1000$, respectively. The sample generation and parameter tuning approach are identical to Section IV.B. The simulation is repeated by 50 times for $S = 100$ and $S = 1000$, respectively. The results are gathered in Table II.

From Table II, it can be observed that the average out-of-sample performance of the proposed DROGPF model is still better than SAA in both $S = 100$ and $S = 1000$ cases, indicating the effectiveness of the proposed methods. However, the average OP improvement rate decreases from 1.546% to 1.120% and 0.300%, respectively, when S increases from 20 to 100 and 1000, suggesting the proposed methods would have similar out-of-sample performance with SAA when the sample set is sufficient large.

5) Computational Efficiency Analysis: In the sequel, we apply the proposed model and algorithm to a larger test system, which comprises a modified IEEE 118-bus power network and a modified version of the Belgian high-calorific 20-node gas network. The power network includes 30 gas-fired generator, 24 non-gas generators, 186 transmission lines and 90 loads. The gas network contains 2 gas wells, 16 passive pipelines, 3 compressors and 9 loads. Refer to [39] for the topology as well as parameters of the test system, the working status of generators, load demands and forecasted wind generation outputs curves. According to Section II. B, the number of auxiliary linear constraints generated during the dualization of the expectation of the maximization term in (21a), which is the major computational burden of the proposed DROGPF model, is not related with the number of wind farms. Therefore, 3 wind farms rather than more are considered in the test system. Hereinafter, the test system is referred to as the Power118Gas20 system.

Three sizes of sample sets are prepared for the proposed DROGPF model and the benchmark SAA approach, which are $S = 20$, $S = 50$, and $S = 100$, respectively. The simulations are repeated 100 times for each sample set size setting. The simulation environment, solver settings, as well as algorithmic parameters are identical to previous ones. The results are summarized in Table III, where ACP is short for average computational performance.

From Table III, the average out-of-sample performance of the proposed DROGPF model is still better than SAA for the Power118Gas20 system, indicating the effectiveness of the proposed methods. Similar with the results in Table II, the gap between the performances of the proposed DROGPF and SAA gets smaller while the sample dataset size grows. The 4^{th} to 7^{th} column of Table III describe the numbers of auxiliary variables and constraints in the proposed DROGPF and SAA models, while the other decision variables and constraints of the two models are the same. It should be noted that L_e^* in Table III is the number of active transmission lines in the power network after inactive transmission capacity constraints identification [40]. The average total computational time as well as algorithmic iteration number are demonstrated in the last two columns of Table III. It can be observed that the computational time almost grow linearly with respect to the

TABLE III
COMPARISON OF THE PROPOSED DROGPF MODEL AND SAA FOR THE POWER118GAS20 SYSTEM.

Model type	Sample Number	Average OP ($)	Auxiliary variables		Auxiliary linear constraints		ACP	
			General expression	Number	General expression	Number	Time (s)	Iteration
DROGPF	$S=20$	8.8923×10^6	$(2G+2N+L_e^*)\times(S+1)\times T$	96264	$(4G+4N+3L_e^*)\times S\times T$ $+(2G+2N+L_e^*)\times T$	227784	265.3	7.85
	$S=50$	8.8272×10^6		233784		562584	523.7	8.13
	$S=100$	8.5464×10^6		462984		1120584	1481	8.21
SAA	$S=20$	9.0851×10^6	$(2G+2N+L_e^*)\times S\times T$	91680	$(4G+4N+3L_e^*)\times S\times T$	223200	260.5	7.79
	$S=50$	8.9725×10^6		229200		558000	519.8	8.14
	$S=100$	8.5885×10^6		458400		1116000	1447	8.19

size of sample dataset, as the additional auxiliary constraints are linear and their number grow linearly along with the size of sample dataset. Moreover, the average iteration number does not increase much as the sample number increases from the simulation results. In fact, the necessity of the iterations is to tighten the convex relaxation for the Weymouth equations in the gas network and gradually turn an infeasible solution into a feasible one. The number of Weymouth equations stays unchanged as the sample number rises, making the algorithmic iteration number insensitive to the size of sample dataset. In addition, the computational time for the Power118Gas20 system with 100 samples is less than 25 minutes, which is acceptable for the 24-period scheduling problem of a moderate size test system.

V. CONCLUSION

With the increasing penetration level of uncertain wind generation in power systems, OGPF calculation in an uncertain environment is desired, as the interactions between power systems and gas systems have been significantly enhanced in recent decades. In this regard, the risk-based DROGPF model is proposed, where the distributional uncertainty set is constructed based on Wasserstein distance. Influences of reserves from gas-fired units on the economic and secure operation of the gas system are quantified by proposing the concept of zonal line pack, which originates from the heterogeneity of gas and electricity, as well as adding constraints to limit the reserve commitment of gas-fired unit from the perspective of the gas system. An iterative solution procedure for the proposed DROGPF model is designed based on convex optimization, where SOCPs are solved in each iteration. Simulation results on the test system reveals the effectiveness and prospects of the proposed models and methods on out-of-sample performances, computational costs, and practicality. Future works include developing a non-cooperative fully distributed decision-making framework as well as replacing the affine policy reserve utilization rule with a fully dispatchable one for the coupled electricity-gas system.

APPENDIX

A. Detailed Expressions of Coefficients

The index set $\{1,\dots,K\}$ is reparameterized as

$$\Big\{(j_{d_e}^{gt},j_w^{gt},j_{d_e}^{nt},j_w^{nt},j_{l_e}^{t}): j_{d_e}^{gt},j_w^{gt},j_{d_e}^{nt},j_w^{nt}\in\{1,2\},$$
$$j_{l_e}^{t}\in\{1,2,3\},\ \forall g\in\mathcal{G},l_e\in\mathcal{L}_e,t\in\mathcal{T}\Big\},$$

and thus $K=4^{(G+N)T}\times 3^{L_eT}$. We express

$$\boldsymbol{a}_{(j_{d_e}^{gt},j_w^{gt},j_{d_e}^{nt},j_w^{nt},j_{l_e}^{t})}(\boldsymbol{x})=\sum_{t\in\mathcal{T}}\Big(\sum_{g\in\mathcal{G}}\Big(\boldsymbol{a}_{j_{d_e}^{gt}}^{gt}(\boldsymbol{x})+\boldsymbol{a}_{j_w^{gt}}^{gt}(\boldsymbol{x})\Big)+$$
$$\sum_{n\in\mathcal{N}}\Big(\boldsymbol{a}_{j_{d_e}^{nt}}^{nt}(\boldsymbol{x})+\boldsymbol{a}_{j_w^{nt}}^{nt}(\boldsymbol{x})\Big)+\sum_{l_e\in\mathcal{L}_e}\boldsymbol{a}_{j_{l_e}^{t}}^{l_et}(\boldsymbol{x})\Big),$$

$$b_{(j_{d_e}^{gt},j_w^{gt},j_{d_e}^{nt},j_w^{nt},j_{l_e}^{t})}(\boldsymbol{x})=\sum_{t\in\mathcal{T}}\Big(\sum_{g\in\mathcal{G}}\Big(b_{j_{d_e}^{gt}}^{gt}(\boldsymbol{x})+b_{j_w^{gt}}^{gt}(\boldsymbol{x})\Big)+$$
$$\sum_{n\in\mathcal{N}}\Big(b_{j_{d_e}^{nt}}^{nt}(\boldsymbol{x})+b_{j_w^{nt}}^{nt}(\boldsymbol{x})\Big)+\sum_{l_e\in\mathcal{L}_e}b_{j_{l_e}^{t}}^{l_et}(\boldsymbol{x})\Big),$$

where $\boldsymbol{a}_{j_{d_e}^{gt}}^{gt}(\boldsymbol{x})$, $\boldsymbol{a}_{j_w^{gt}}^{gt}(\boldsymbol{x})$, $\boldsymbol{a}_{j_{d_e}^{nt}}^{nt}(\boldsymbol{x})$, $\boldsymbol{a}_{j_w^{nt}}^{nt}(\boldsymbol{x})$, $\boldsymbol{a}_{j_{l_e}^{t}}^{l_et}(\boldsymbol{x})$, $b_{j_{d_e}^{gt}}^{gt}(\boldsymbol{x})$, $b_{j_w^{gt}}^{gt}(\boldsymbol{x})$, $b_{j_{d_e}^{nt}}^{nt}(\boldsymbol{x})$, $b_{j_w^{nt}}^{nt}(\boldsymbol{x})$, $b_{j_{l_e}^{t}}^{l_e}(\boldsymbol{x})$ are defined through

$$\boldsymbol{a}_{j_{d_e}^{gt}}^{gt}(\boldsymbol{x})^\top\boldsymbol{\xi}=\begin{cases}-\beta_{d_e}\alpha_{gt}\sum_{w\in\mathcal{W}}\tilde{p}_{wt}, & j_{d_e}^{gt}=1,\\ 0, & j_{d_e}^{gt}=2,\end{cases}$$

$$\boldsymbol{a}_{j_w^{gt}}^{gt}(\boldsymbol{x})^\top\boldsymbol{\xi}=\begin{cases}\beta_{w}\alpha_{gt}\sum_{w\in\mathcal{W}}\tilde{p}_{wt}, & j_{w}^{gt}=1,\\ 0, & j_{w}^{gt}=2,\end{cases}$$

$$\boldsymbol{a}_{j_{d_e}^{nt}}^{nt}(\boldsymbol{x})^\top\boldsymbol{\xi}=\begin{cases}-\beta_{d_e}\alpha_{nt}\sum_{w\in\mathcal{W}}\tilde{p}_{wt}, & j_{d_e}^{nt}=1,\\ 0, & j_{d_e}^{nt}=2,\end{cases}$$

$$\boldsymbol{a}_{j_w^{nt}}^{nt}(\boldsymbol{x})^\top\boldsymbol{\xi}=\begin{cases}\beta_{w}\alpha_{nt}\sum_{w\in\mathcal{W}}\tilde{p}_{wt}, & j_{w}^{nt}=1,\\ 0, & j_{w}^{nt}=2,\end{cases}$$

$$b_{j_{d_e}^{gt}}^{gt}(\boldsymbol{x})=\begin{cases}-\beta_{d_e}\begin{pmatrix}\eta_g\sum_{l_g\in\Psi_{l_g}(g)}m_{l_gt}^{g,+}/\sigma\\ -\alpha_{gt}\sum_{w\in\mathcal{W}}p_{wt}\end{pmatrix}, & j_{d_e}^{gt}=1,\\ 0, & j_{d_e}^{gt}=2,\end{cases}$$

$$b_{j_w^{gt}}^{gt}(\boldsymbol{x})=\begin{cases}-\beta_{w}\begin{pmatrix}\eta_g\sum_{l_g\in\Psi_{l_g}(g)}m_{l_gt}^{g,-}/\sigma\\ +\alpha_{gt}\sum_{w\in\mathcal{W}}p_{wt}\end{pmatrix}, & j_{w}^{gt}=1,\\ 0, & j_{w}^{gt}=2,\end{cases}$$

$$b_{j_{d_e}^{nt}}^{nt}(\boldsymbol{x})=\begin{cases}-\beta_{d_e}\left(r_{nt}^{+}-\alpha_{nt}\sum_{w\in\mathcal{W}}p_{wt}\right), & j_{d_e}^{nt}=1,\\ 0, & j_{d_e}^{nt}=2,\end{cases}$$

$$b_{j_w^{nt}}^{nt}(\boldsymbol{x})=\begin{cases}-\beta_{w}\left(r_{nt}^{-}+\alpha_{nt}\sum_{w\in\mathcal{W}}p_{wt}\right), & j_{w}^{nt}=1,\\ 0, & j_{w}^{nt}=2,\end{cases}$$

$$\boldsymbol{a}_{j_{l_e}^t}^{l_e t}(\boldsymbol{x})^\top \boldsymbol{\xi} =$$
$$\begin{cases} \beta_{l_e} \left(\begin{array}{c} \sum\limits_{w\in\mathcal{W}} \pi_{wl_e}\tilde{p}_{wt} - \sum\limits_{g\in\mathcal{G}} \pi_{gl_e}\alpha_{gt} \sum\limits_{w\in\mathcal{W}} \tilde{p}_{wt} \\ - \sum\limits_{n\in\mathcal{N}} \pi_{nl_e}\alpha_{nt} \sum\limits_{w\in\mathcal{W}} \tilde{p}_{wt} \end{array} \right), & j_{l_e}^t = 1, \\ \beta_{l_e} \left(\begin{array}{c} \sum\limits_{g\in\mathcal{G}} \pi_{gl_e}\alpha_{gt} \sum\limits_{w\in\mathcal{W}} \tilde{p}_{wt} - \sum\limits_{w\in\mathcal{W}} \pi_{wl_e}\tilde{p}_{wt} \\ + \sum\limits_{n\in\mathcal{N}} \pi_{nl_e}\alpha_{nt} \sum\limits_{w\in\mathcal{W}} \tilde{p}_{wt} \end{array} \right), & j_{l_e}^t = 2, \\ 0, & j_{l_e}^t = 3, \end{cases}$$

$$b_{j_{l_e}^t}^{l_e t}(\boldsymbol{x}) =$$
$$\begin{cases} \beta_{l_e} \left(\begin{array}{c} \sum_{g\in\mathcal{G}} \pi_{gl_e}\Big(p_{gt} + \alpha_{gt}\sum_{w\in\mathcal{W}} p_{wt}\Big) \\ + \sum_{n\in\mathcal{N}} \pi_{nl_e}\Big(p_{nt} + \alpha_{nt}\sum_{w\in\mathcal{W}} p_{wt}\Big) \\ - \sum_{d_e\in\mathcal{D}_e} \pi_{d_e l_e} p_{d_e t} - p_{l_e} \end{array} \right) & j_{l_e}^t = 1, \\ \beta_{l_e} \left(\begin{array}{c} -\sum_{g\in\mathcal{G}} \pi_{gl_e}\Big(p_{gt} + \alpha_{gt}\sum_{w\in\mathcal{W}} p_{wt}\Big) \\ - \sum_{n\in\mathcal{N}} \pi_{nl_e}\Big(p_{nt} + \alpha_{nt}\sum_{w\in\mathcal{W}} p_{wt}\Big) \\ + \sum_{d_e\in\mathcal{D}_e} \pi_{d_e l_e} p_{d_e t} - p_{l_e} \end{array} \right) & j_{l_e}^t = 2, \\ 0, & j_{l_e}^t = 3. \end{cases}$$

B. Auxiliary Constraints Reduction

Equivalent forms of (23b) and y_s in (23a) are given as follows.

$$\begin{aligned} y_s^{gtd_e} &\geq \boldsymbol{a}_{j_{d_e}^{gt}}^{gt}(\boldsymbol{x})^\top \hat{\boldsymbol{\xi}}^s + b_{j_{d_e}^{gt}}^{gt}(\boldsymbol{x}),\ \forall t\in\mathcal{T}, g\in\mathcal{G}, \forall j_{d_e}^{gt}, \\ y_s^{gtw} &\geq \boldsymbol{a}_{j_w^{gt}}^{gt}(\boldsymbol{x})^\top \hat{\boldsymbol{\xi}}^s + b_{j_w^{gt}}^{gt}(\boldsymbol{x}), \forall t\in\mathcal{T}, g\in\mathcal{G}, \forall j_w^{gt}, \\ y_s^{ntd_e} &\geq \boldsymbol{a}_{j_{d_e}^{nt}}^{nt}(\boldsymbol{x})^\top \hat{\boldsymbol{\xi}}^s + b_{j_{d_e}^{nt}}^{nt}(\boldsymbol{x}), \forall t\in\mathcal{T}, n\in\mathcal{N}, \forall j_{d_e}^{nt}, \\ y_s^{ntw} &\geq \boldsymbol{a}_{j_w^{nt}}^{nt}(\boldsymbol{x})^\top \hat{\boldsymbol{\xi}}^s + b_{j_w^{nt}}^{nt}(\boldsymbol{x}), \forall t\in\mathcal{T}, n\in\mathcal{N}, \forall j_w^{nt}, \\ y_s^{l_e t} &\geq \boldsymbol{a}_{j_{l_e}^t}^{l_e t}(\boldsymbol{x})^\top \hat{\boldsymbol{\xi}}^s + b_{j_{l_e}^t}^{l_e t}(\boldsymbol{x}),\ \forall t\in\mathcal{T}, l_e\in\mathcal{L}_e, \forall j_{l_e}^t. \end{aligned}$$

$$y_s = \sum_{t\in\mathcal{T}} \Big(\sum_{g\in\mathcal{G}} (y_s^{gtd_e} + y_s^{gtw}) + \sum_{n\in\mathcal{N}} (y_s^{ntd_e} + y_s^{ntw}) + \sum_{l_e\in\mathcal{L}_e} y_s^{l_e t} \Big),\ \forall s\in\mathcal{S}.$$

REFERENCES

[1] "World energy look 2013," International Energy Agency, Paris, France, 2013.

[2] M. Gtz, J. Lefebvre, F. Mrs, A. M. Koch, F. Graf, S. Bajohr, R. Reimert, and T. Kolb, "Renewable Power-to-Gas: A technological and economic review," *Renewable Energy*, vol. 85, pp. 1371 – 1390, 2016.

[3] C. Liu, M. Shahidehpour, Y. Fu, and Z. Li, "Security-constrained unit commitment with natural gas transmission constraints," *IEEE Trans. on Power Syst.*, vol. 24, no. 3, pp. 1523–1536, Aug 2009.

[4] X. Zhang, M. Shahidehpour, A. S. Alabdulwahab, and A. Abusorrah, "Security-constrained co-optimization planning of electricity and natural gas transportation infrastructures," *IEEE Trans. on Power Syst.*, vol. 30, no. 6, pp. 2984–2993, Nov 2015.

[5] M. Gil, P. Dueas, and J. Reneses, "Electricity and natural gas interdependency: Comparison of two methodologies for coupling large market models within the european regulatory framework," *IEEE Trans. on Power Syst.*, vol. 31, no. 1, pp. 361–369, Jan 2016.

[6] C. Correa-Posada and P. Sánchez-Martin, "Security-constrained optimal power and natural-gas flow," *IEEE Trans. on Power Syst.*, vol. 29, no. 4, pp. 1780–1787, Jul. 2014.

[7] ——, "Integrated power and natural gas model for energy adequacy in short-term operation," *IEEE Trans. on Power Syst.*, vol. 30, no. 6, pp. 3347–3355, Nov. 2015.

[8] H. Cui, F. Li, Q. Hu, L. Bai, and X. Fang, "Day-ahead coordinated operation of utility-scale electricity and natural gas networks considering demand response based virtual power plants," *Appl. Energy*, vol. 6, pp. 183–195, Aug. 2016.

[9] Y. Wen, X. Qu, W. Li, X. Liu, and X. Ye, "Synergistic operation of electricity and natural gas networks via ADMM," *IEEE Trans. on Smart Grid*, vol. 9, no. 5, pp. 4555 – 4565, Sep 2018.

[10] C. Wang, W. Wei, J. Wang, L. Bai, Y. Liang, and T. Bi, "Convex optimization based distributed optimal gas-power flow calculation," *IEEE Trans. on Sustain. Energy*, vol. 9, no. 3, pp. 1145–1156, Jul 2018.

[11] A. Alabdulwahab, A. Abusorrah, X. Zhang, and M. Shahidehpour, "Coordination of interdependent natural gas and electricity infrastructures for firming the variability of wind energy in stochastic day-ahead scheduling," *IEEE Trans. on Sustain. Energy*, vol. 6, no. 2, pp. 606–615, April 2015.

[12] C. He, L. Wu, T. Liu, and M. Shahidehpour, "Robust co-optimization scheduling of electricity and natural gas systems via admm," *IEEE Trans. on Sustain. Energy*, vol. 8, no. 2, pp. 658–670, April 2017.

[13] A. Shapiro, "Distributionally robust stochastic programming," *SIAM Journal on Optimization*, vol. 27, no. 4, pp. 2258–2275, 2017.

[14] P. Xiong, P. Jirutitijaroen, and C. Singh, "A distributionally robust optimization model for unit commitment considering uncertain wind power generation," *IEEE Transactions on Power Systems*, vol. 32, no. 1, pp. 39–49, Jan 2017.

[15] W. Wei, F. Liu, and S. Mei, "Distributionally robust co-optimization of energy and reserve dispatch," *IEEE Trans. on Sustain. Energy*, vol. 7, no. 1, pp. 289–300, Jan 2016.

[16] Y. Zhang, S. Shen, and J. Mathieu, "Distributionally Robust Chance-Constrained Optimal Power Flow with Uncertain Renewables and Uncertain Reserves Provided by Loads," *IEEE Trans. on Power Syst.*, vol. 32, no. 2, pp. 1378–1388, Mar. 2017.

[17] R. Gao and A. J. Kleywegt, "Distributionally robust stochastic optimization with wasserstein distance," *arXiv:1604.02199*, 2016.

[18] S. Clegg and P. Mancarella, "Integrated electrical and gas network flexibility assessment in low-carbon multi-energy systems," *IEEE Trans. on Sustain. Energy*, vol. 7, no. 2, pp. 718–731, April 2016.

[19] Y. He, M. Shahidehpour, Z. Li, C. Guo, and B. Zhu, "Robust constrained operation of integrated electricity- natural gas system considering distributed natural gas storage," *IEEE Trans. on Sustain. Energy*, vol. 9, no. 3, pp. 1061 – 1071, July 2017.

[20] S. Wu, R. Ríos-Mercado, E. Boyd, and L. Scott, "Model relaxations for the fuel cost minimization of steady-state gas pipeline networks," University of Chicago, Tech. Rep., 1999.

[21] A. Tomasgard, F. Rmo, M. Fodstad, and K. Midthun, "Optimization Models for the Natural Gas Value Chain," in *Geometric Modelling, Numerical Simulation, and Optimization: Applied Mathematics at SINTEF*. Berlin, Heidelberg: Springer, 2007, pp. 521–558.

[22] F. Babonneau, Y. Nesterov, and J. Vial, "Design and operations of gas transmission networks," *Oper. Res.*, vol. 60, no. 1, pp. 34–47, 2012.

[23] N. Keyaerts, "Gas balancing and line-pack flexibility," Ph.D. dissertation, KU Leuven, Leuven, Sep. 2012. [Online]. Available: https://www.mech.kuleuven.be/en/tme/research/energy_environment/Pdf/wpen2012-11.pdf

[24] (2018). [Online]. Available: https://en.wikipedia.org/wiki/List_of_United_States_electric_companies

[25] P. Weigand, G. Lander, and R. Malme, "Synchronizing natural gas & power market: a series of proposed solutions," Skipping Stone, Tech. Rep., Jan. 2013.

[26] R. A. Jabr, "Adjustable robust opf with renewable energy sources," *IEEE Trans. on Power Syst.*, vol. 28, no. 4, pp. 4742–4751, Nov 2013.

[27] Y. Wang, S. Zhao, Z. Zhou, A. Botterud, Y. Xu, and R. Chen, "Risk adjustable day-ahead unit commitment with wind power based on chance constrained goal programming," *IEEE Trans. on Sustain. Energy*, vol. 8, no. 2, pp. 530–541, April 2017.

[28] Z. Wang, Q. Bian, H. Xin, and D. Gan, "A distributionally robust coordinated reserve scheduling model considering cvar-based wind power reserve requirements," *IEEE Trans. on Sustain. Energy*, vol. 7, no. 2, pp. 625–636, April 2016.

[29] C. Duan, W. Fang, L. Jiang, L. Yao, and J. Liu, "Distributionally robust chance-constrained approximate ac-opf with wasserstein metric," *IEEE Transactions on Power Systems*, vol. 33, no. 5, pp. 4924–4936, Sept 2018.

[30] N. Jaleeli, L. S. VanSlyck, D. N. Ewart, L. H. Fink, and A. G. Hoffmann, "Understanding automatic generation control," *IEEE Transactions on Power Systems*, vol. 7, no. 3, pp. 1106–1122, Aug 1992.

[31] C. Zhao and R. Jiang, "Distributionally robust contingency-constrained unit commitment," *IEEE Transactions on Power Systems*, vol. 33, no. 1, pp. 94–102, Jan 2018.

[32] R. Gao, L. Xie, Y. Xie, and H. Xu, "Robust Hypothesis Testing Using Wasserstein Uncertainty Sets," *arXiv:1805.10611 [cs, math, stat]*, May 2018, arXiv: 1805.10611. [Online]. Available: http://arxiv.org/abs/1805.10611
[33] P. M. Esfahani and D. Kuhn, "Data-driven distributionally robust optimization using the wasserstein metric: Performance guarantees and tractable reformulations," *arXiv:1505.05116*, 2015.
[34] C. Zhao and Y. Guan, "Data-driven stochastic unit commitment for integrating wind generation," *IEEE Transactions on Power Systems*, vol. 31, no. 4, pp. 2587–2596, July 2016.
[35] Z. Li, W. Wu, B. Zhang, and X. Tai, "Kullbackleibler divergence-based distributionally robust optimisation model for heat pump day-ahead operational schedule to improve pv integration," *IET Generation, Transmission Distribution*, vol. 12, no. 13, pp. 3136–3144, 2018.
[36] P. Mohajerin Esfahani and D. Kuhn, "Data-driven distributionally robust optimization using the Wasserstein metric: performance guarantees and tractable reformulations," *Mathematical Programming*, vol. 171, no. 1, pp. 115–166, 2018.
[37] F. Alizadeh and D. Goldfarb, "Second-order cone programming," *Math. Prog.*, vol. 95, pp. 3–51, Jan. 2003.
[38] T. Lipp and S. Boyd, "Variations and extension of the convex-concave procedure," *Optim. Eng.*, vol. 17, pp. 263–287, 2016.
[39] (2018). [Online]. Available: https://sites.google.com/site/chengwang0617/home/data-sheet
[40] H. Ye and Z. Li, "Necessary conditions of line congestions in uncertainty accommodation," *IEEE Transactions on Power Systems*, vol. 31, no. 5, pp. 4165–4166, Sept 2016.

Cheng Wang (M'18) received the B.Sc. and Ph.D. degrees in electrical engineering from Tsinghua University, Beijing, China, in 2012 and 2017, respectively.

Dr. Wang was a Visiting Ph.D. student at Argonne National Laboratory, Argonne, IL, USA, from 2015 to 2016. He is currently a Lecturer with North China Electric Power University, Beijing, China. His research interests include optimization and control of integrated energy systems.

Rui Gao received his BSc in Mathematics and Applied Mathematics from Xi'an Jiaotong University, Xi'an, China, in 2013, and his PhD in Operations Research from Georgia Institute of Technology, Atlanta, USA, in 2018. He is currently an Assistant Professor with University of Texas at Austin, Austin, USA. His research interests are in data-driven decision-making under uncertainty, statistical learning, and their applications in power systems.

Wei Wei (M'15-SM'18) received the B.Sc. and Ph.D. degrees in electrical engineering from Tsinghua University, Beijing, China, in 2008 and 2013, respectively.

Dr. Wei was a Postdoctoral Research Fellow with Tsinghua University from 2013 to 2015. He was a Visiting Scholar with Cornell University, Ithaca, NY, USA, in 2014, and with Harvard University, Cambridge, MA, USA, in 2015. He is currently an Associate Professor with Tsinghua University. His research interests include applied optimization and energy economics.

Miadreza Shafie-khah (M'13-SM'17) received the M.Sc. and Ph.D. degrees in electrical engineering from Tarbiat Modares University, Tehran, Iran, in 2008 and 2012, respectively. He received his first postdoc from the University of Beira Interior (UBI), Covilha, Portugal in 2015, while working on the 5.2-million-euro FP7 project SiNGULAR ("Smart and Sustainable Insular Electricity Grids Under Large-Scale Renewable Integration"). He received his second postdoc from the University of Salerno, Salerno, Italy in 2016. He was considered one of the Outstanding Reviewers of the IEEE TRANSACTIONS ON SUSTAINABLE ENERGY, in 2014 and 2017, one of the Best Reviewers of the IEEE TRANSACTIONS ON SMART GRID, in 2016 and 2017, and one of the Outstanding Reviewers of the IEEE TRANSACTIONS ON POWER SYSTEMS, in 2017. His research interests include power market simulation, market power monitoring, power system optimization, demand response.

Tianshu Bi (M'98-SM'09) received her Ph.D. degree at the Department of EEE in the University of Hong Kong in 2002. She is currently a professor at North China Electric Power University.

Her research interests include power system protection and control, synchronized phasor measurement technique and its application and fault diagnose.

João P. S. Catalão (M'04-SM'12) received the M.Sc. degree from the Instituto Superior Técnico (IST), Lisbon, Portugal, in 2003, and the Ph.D. degree and Habilitation for Full Professor ("Agregacão") from the University of Beira Interior (UBI), Covilha, Portugal, in 2007 and 2013, respectively.

Currently, he is a Professor at the Faculty of Engineering of the University of Porto (FEUP), Porto, Portugal, and Researcher at INESC TEC, INESC-ID/IST-UL, and C-MAST/UBI. He was also appointed as Visiting Professor by North China Electric Power University, Beijing, China. He was the Primary Coordinator of the EU-funded FP7 project SiNGULAR ("Smart and Sustainable Insular Electricity Grids Under Large-Scale Renewable Integration"), a 5.2-million-euro project involving 11 industry partners. He has authored or coauthored more than 675 publications, including 252 journal papers (more than 75 IEEE Transactions/Journal papers), 370 conference proceedings papers, 5 books, 34 book chapters, and 14 technical reports, with an h-index of 45, an i10-index of 178, and over 7700 citations (according to Google Scholar), having supervised more than 70 post-docs, Ph.D. and M.Sc. students. He is the Editor of the books entitled "Electric Power Systems: Advanced Forecasting Techniques and Optimal Generation Scheduling" and "Smart and Sustainable Power Systems: Operations, Planning and Economics of Insular Electricity Grids" (Boca Raton, FL, USA: CRC Press, 2012 and 2015, respectively). His research interests include power system operations and planning, hydro and thermal scheduling, wind and price forecasting, distributed renewable generation, demand response and smart grids.

Prof. Catalão is an Editor of the IEEE TRANSACTIONS ON SMART GRID, an Editor of the IEEE TRANSACTIONS ON POWER SYSTEMS, an Associate Editor of the IEEE TRANSACTIONS ON INDUSTRIAL INFORMATICS, and a Subject Editor of the IET Renewable Power Generation. From 2011 till 2018 (seven years) he was an Editor of the IEEE TRANSACTIONS ON SUSTAINABLE ENERGY and an Associate Editor of the IET Renewable Power Generation. He was the Guest Editor-in-Chief for the Special Section on "Real-Time Demand Response" of the IEEE TRANSACTIONS ON SMART GRID, published in December 2012, the Guest Editor-in-Chief for the Special Section on "Reserve and Flexibility for Handling Variability and Uncertainty of Renewable Generation" of the IEEE TRANSACTIONS ON SUSTAINABLE ENERGY, published in April 2016, and the Corresponding Guest Editor for the Special Section on "Industrial and Commercial Demand Response" of the IEEE TRANSACTIONS ON INDUSTRIAL INFORMATICS, published in November 2018. Since March 2018, he is the Lead Guest Editor for the Special Issue on "Demand Side Management and Market Design for Renewable Energy Support and Integration" of the IET Renewable Power Generation. He was the recipient of the 2011 Scientific Merit Award UBI-FE/Santander Universities, the 2012 Scientific Award UTL/Santander Totta, the 2016 FEUP Diploma of Scientific Recognition, and the Best INESC-ID Researcher 2017 Award, in addition to an Honorable Mention in the 2017 Scientific Awards ULisboa/Santander Universities. Moreover, he has won 4 Best Paper Awards at IEEE Conferences.